Investigation of Wavelength Conversion by Four-Wave Mixing in Semiconductor Optical Amplifiers

Thesis by

David Francis Geraghty

In Partial Fulfillment of the Requirements

for the Degree of

Doctor of Philosophy

California Institute of Technology

Pasadena, California

1997

(Defended April 29, 1997)

For My Parents

And For Sarah

Acknowledgments

There are so many people that I need to acknowledge, it hardly seems right to call this my thesis. The person deserving the greatest acknowledgment for my succesful completion of this thesis is my advisor, Prof. Kerry J. Vahala. I knew that he was something special as an instructor and a mentor ever since my junior year in his quantum class. Without his guidance and assistance, this work would not have been possible.

Robert Lee has done more than I can possibly acknowledge, working "side-by-side" with me for the last 2 years.

Current graduate students Guido Hunziker and Roberto Paiella also need acknowledgment. They did the background work on the polarization insensitive demonstration, and then performed the systems-level experiment with me. But also, and almost more importantly, they have made the lab a fun place to work.

I also need to thank a few of the graduate students in the group that came before me: Dr. Jay Dawson, Dr. Namkyoo Park, Dr. Charles Tsai and Dr. Jianhui Zhou. Jay and Namkyoo really helped out getting me started when I first arrived for graduate school. Namkyoo also helped with the measurements characterizing the microcavity laser. Charles seemed to always know the answers to the fundamental questions, like how big of a resistor to use. Jianhui was invaluable. Initially for establishing the group's effort in this area, and then for working with me on the beginning of the systems-level work, also, and mainly, for being a great scientist and mentor. His achievement and attitude towards scientific endeavors is something I

strive for, and he also is a great motivator and supporter.

Many people have donated time or equipment for the effort. Dr. Thomas Schrans and Dr. Norman Kwong at Ortel provided invaluable assistance and equipment to get the 10 Gb/s system up and running and understood. Dr. Al Benzoni's help with the TRSA experiment was great. Uzi Koren at Lucent Technologies and our friends at SDL supplied us with SOAs, without which this work could not have been done. And Tom Veegers and Northrop must be acknowledged for the extra Amoco EDFA for the cascade experiments.

Outside of lab, I must also acknowledge a few people. Uncle Pat and his occasional nickel helped make grad school more palatable. My brothers and sisters gave me a lot of support, and also a lot of nieces and nephews who were fun to visit and helped keep life in perspective as to what is really important. My parents. From the beginning there has been love, support, guidance, and milk shake money for everything I have tried.

And finally Sarah. I can't say enough, so I'm afraid to try. I'm sure that without her I would not be at this point.

Abstract

Four-wave mixing (FWM) in semiconductor optical amplifiers (SOAs) is investigated for wavelength conversion in high-speed, all-optical networks. The design of the wavelength converter is optimized and the system performance limitations imposed by the fundamental physical principles involved in the SOA FWM process are characterized.

Single channel conversion performance is evaluated. The FWM efficiency ultimately determines many systems-level characteristics of the wavelength converter. The spectral range of our wavelength converter is characterized. Wide wavelength conversions of up to 18 nm and complete coverage of a 10 nm spectral range are demonstrated, while maintaining a BER performance of better than 10^{-9} at 10 Gb/s. The converter also demonstrates a large dynamic input range of over 10 dB at 2.5 Gb/s. And the first characterization of cascaded FWM SOA wavelength converters, cascading conversion of up to 10 nm at 10 Gb/s, is performed.

With a simple modification of the converter design to a dual-pump configuration, the wavelength converter is able to provide nearly polarization insensitive performance. The converted signal's magnitude varies by less than 1.5 dB and its sensitivity varies by less than 2 dB for 2.5 Gb/s signals over the entire range of input polarizations.

Time resolved spectral analysis is performed to evaluate the spectral properties of the wavelength converter. A pattern-dependent additional chirp is measured on the signal, primarily resulting from fluctuations in the gain saturation of the SOA. This

degradation to the optical phase conjugation, intrinsic to the SOA FWM process, is minimal enough to allow dispersion compensation by mid-span spectral inversion. Error-free detection of a directly modulated 10 Gb/s signal is achieved over 120 km.

Additional demonstrations are also presented. Multi-channel wavelength conversion and dynamic routing are successfully performed. Finally, some work on a micro-cavity erbium-doped fiber laser, initially designed and developed for use as a tunable source for wavelength-division multiplexed networks, is presented.

Contents

List of Figures

Chapter 1

Introduction

Historically, optical fiber communication networks have been single channel, point-to-point links. Current state-of-the-art commercial links utilize wavelength division multiplexing (WDM), however they are still simple networks with most of the network functions implemented electrically. Much research is being done towards future fiber communication systems that are all-optical, with all network functions performed optically [1, 2, 3]. Many demonstrations have already performed various networking functions without an optical-electronic-optical conversion, such as dynamic routing [4], bit phase sensing [5], and packet header recognition [6]. There are many potential mechanisms for the implementation of all-optical wavelength conversion [7]. The work presented here in this thesis, presented elsewhere in [8, 9, 10, 11, 12, 13, 14, 15, 16, 17, 18], describes the characterization of the performance of a four-wave mixing (FWM) semiconductor optical amplifier (SOA) wavelength converter in a high-speed optical communications link.

The non-linear properties of SOAs have been well characterized. In Chapter 2,

I present a summary of the theoretical background necessary to understand the capabilities and limitations of a FWM SOA wavelength converter. The mechanisms involved in the FWM process are first discussed. Then a simple model predicting the FWM conversion efficiency is presented.

The design of the FWM SOA wavelength converter is presented in Chapter 3. I first describe the physical elements utilized. Then the operating parameters and specific design issues are discussed in further detail. Finally, I present some work on a design modification that may prove optimal for further work.

The single channel performance of the FWM SOA wavelength converter in a point-to-point optical communications link is presented in Chapter 4. The spectral range of the converter is characterized at 10 Gb/s, and the dynamic input range of the converter is characterized at 2.5 Gb/s.

Chapter 5 presents work on issues critical for implementation of the converter in a real system. The performance of two cascaded wavelength converters is analyzed, and a model is presented to predict the absolute cascadability of the converters. Additionally, work on polarization independent converter performance is presented. A mechanism that allows nearly polarization-independent performance is introduced. The modifications required of the converter design are discussed. And finally the polarization sensitivity of the converter performance is analyzed.

The spectral properties of the wavelength converter are investigated in Chapter 6. Time resolved spectral analysis is performed to evaluate the effect of the wavelength converter on the chirp of the signal. Additionally, dispersion compensation in optical

fibers is demonstrated by mid-span spectral inversion, utilizing the optical phase conjugation of the FWM SOA wavelength converter.

A few additional demonstrations are presented in Chapter 7. The performance of the FWM SOA wavelength converter is evaluated under multi-channel operation, and dynamic channel routing is achieved using the converter. In Chapter 8, I present some additional work on the development of a microcavity erbium-doped fiber laser, a source developed for application in WDM communications systems. And in the appendix, I explain components of the converter performance evaluation process in greater detail.

Bibliography

[1] R. S. Vodhanel, *et al.* , "National scale WDM networking demonstration by the MONET consortium," *Optical Fiber Communication Conference*, Dallas, Texas, February 16-21, 1997, paper PD27.

[2] B. R. Hemenway, M. L. Stevens, R. A. Barry, C. E. Koskal, and E. A. Swanson, "Demonstration of a re-configurable wavelength-routed network at 1.14 terabits-per-second," *Optical Fiber Communication Conference*, Dallas, Texas, February 16-21, 1997, paper PD26.

[3] R. T. Hofmeister, S. M. Gemelos, C. L. Lu, M. C. Ho, D. Wonglumson, D. T. Mayweather, S. Agrawal, and I. Fishman, "Project LEARN–light exchangeable, add/drop ring network," *Optical Fiber Communication Conference*, Dallas, Texas, February 16-21, 1997, paper PD25.

[4] D. Cotter, J. K. Lucek, M. Shabeer, K. Smith, D. C. Rogers, D. Nesset, and P. Gunning, "Self-outing of 100 Gbit/s packets using 6 bit keyword address recognition," *Electron. Lett.*, vol. 31, pp. 2201-2202, 1995.

[5] K. L. Hall, K. A. Rauschenbach, E. A. Swanson, S. R. Chinn, and G. Raybon, "Picosecond-accuracy all-optical bit phase sensing using a nonlinear optical loop mirror," *IEEE Phot. Tech. Lett.*, vol. 7, pp. 935-937, 1995.

[6] E. Park, D. Norte, and A. E. Wilner, "Simultaneous all-optical packet-header replacement and wavelength shifting for a dynamically-reconfigurable WDM network," *IEEE Phot. Tech. Lett.*, vol. 7, pp. 810-812, 1995.

[7] S. J. B. Yoo, "Wavelength conversion technologies for WDM network applications," *J. Light. Tech.*, vol. 14, pp. 955-966, 1996.

[8] D. F. Geraghty, R. B. Lee, K. J. Vahala, M. Verdiell, M. Ziari, and A. Mathur,"Wavelength conversion up to 18 nm at 10 Gb/s by four-wave mixing in a semiconductor optical amplifier," *IEEE Phot. Tech. Lett.*, vol. 9, pp. 452-454, 1997.

[9] D. F. Geraghty, R. B. Lee, and K. J. Vahala,"Cascaded wavelength conversions using four-wave mixing in semiconductor optical amplifiers," *Optical Fiber Communication Conference*, Dallas, Texas, February 16-21, 1997, paper WH6.

[10] D. F. Geraghty, R. B. Lee, K. J. Vahala, M. Verdiell, M. Ziari, and A. Mathur, "Time resolved spectral analysis of phase conjugation by four-wave mixing in semiconductor optical amplifiers," *Conference on Lasers and Electro-Optics*, Baltimore, Maryland, May 18-23, 1997, paper CTuH6.

[11] D. F. Geraghty, R. B. Lee, and K. J. Vahala, "Cascaded wavelength conversions by four-wave mixing in semiconductor optical amplifiers at 10 Gb/s," *OSA Trends in Optics and Photonics Series*, vol. 12, 1997.

[12] K. J. Vahala, J. Zhou, D. Geraghty, R. Lee, M. Newkirk, and B. Miller, "Four-wave mixing in semiconductor traveling-wave amplifiers for wavelength conversion in all-optical networks", *Int. J. of High Speed Elec. and Sys.*, vol. 7, pp. 153-177, 1996.

[13] G. Hunziker, R. Paiella, D. F. Geraghty, K. J. Vahala, and U. Koren, "Polarization-independent wavelength conversion at 2.5 Gb/s by dual-pump four-wave mixing in a strained semiconductor optical amplifier," *IEEE Phot. Tech. Lett.*, vol. 8, pp. 1633-35, 1996.

[14] K. J. Vahala, J. Zhou, D. F. Geraghty, R. B. Lee, M. Newkirk, and B. Miller,"Wavelength shifting by four-wave mixing in semiconductor optical amplifiers," *IEEE Lasers and Electro-Optics Society 1995 Annual Meeting*, October 30-November 2, 1995, paper OC4.2.

[15] R. B. Lee, D. F. Geraghty, K. J. Vahala, and U. Koren, "Cascaded wavelength conversion by four-wave mixing in a strained semiconductor optical amplifier at 10 Gb/s," *IEEE Phot. Tech. Lett.*, vol. 9, 1997.

[16] R. B. Lee, D. F. Geraghty, P. O. Hedekvist, K. J. Vahala, M. Verdiell, M. Ziari and A. Mathur, "Crosstalk penalty in 2-channel wavelength conversion by four-

wave mixing in a strained semiconductor optical amplifier," *Optical Fiber Communication Conference*, Dallas, Texas, February 16-21, 1997, paper WL53.

[17] K. .J Vahala, D. F. Geraghty, R. B. Lee, J. Zhou, M. . Newkirk, and B. .I Miller, "Application of terahertz dynamics in semiconductor optical amplifiers to wavelength conversion in WDM systems," *Photonics West OE/LASE '96*, San Jose, California, February 1-2, 1996, paper 2684-01.

[18] K. J. Vahala, R. B. Lee, D. F. Geraghty, P. O. Hedekvist, J. Zhou, and U. Koren, "Four-wave mixing in semiconductor optical amplifiers for application to ultra-fast wavelength conversion," *Optoelectronics and Communications Conference*, Chiba, Japan, July 16-19, 1996, paper 18D2-1.

Chapter 2

Wavelength Conversion by Four-Wave Mixing in Semiconductor Optical Amplifiers

2.1 Motivation For Wavelength Converters

There is an undeniable reformation occurring in telecommunications today. Suddenly, much to the surprise of McKinsey and AT&T, everyone needs to have a cell phone at their side. Over forty channels of fodder on conventional cable TV can no longer satisfy the daytime talk show junkie; there is now a call for HDTV on demand. And additionally there is the information super-highway; the world-wide web was originally developed for the dissemination of information between scientists, but it is now rapidly becoming the domain of everyone, even those without a computer thanks to Web TV.

As these new applications for telecommunications mature, a greater demand is placed on the bandwidth of the existing telecommunications infrastructure. The demand is rapidly outgrowing the existing capacity. Single-mode fiber installed around the world has the capacity of many Tb/s. However, this capacity is drastically underutilized. Current state-of-the-art systems operate at only 2.5 or 10 Gb/s, allowing for much more efficient use of the bandwidth of the existing infrastructure. Further increasing the single channel speed of these systems to make greater use of the available bandwidth can cause many problems: the cost of the supporting electronics generally goes up as the square-root of the speed [1], and the achievable transmission distance due to dispersion in fibers decreases with increasing speed.

A world-wide consensus is emerging on the utilization of wavelength-division multiplexing (WDM) technologies for a more cost effective use of the available bandwidth [2]. What is being envisioned, and already demonstrated [3, 4, 5], are complex all-optical WDM networks, free of electronic bottlenecks, which can easily handle the demands of today and which can be easily upgraded in the future as new technologies emerge to handle unforeseen demands.

A generic all-optical, WDM optical network is shown in Figure 2.1. Groups of LANs are linked by metropolitan area networks (MANs), with the various MANs linked by a wide-area network (WAN) trunk line. Interconnection schedulers control the flow of traffic between the levels. For a system to reach its full potential, there are many criteria it must meet. First, it must be scalable in its number of end users, number of layers, and supported data rates. It also should be flexible, dynamically

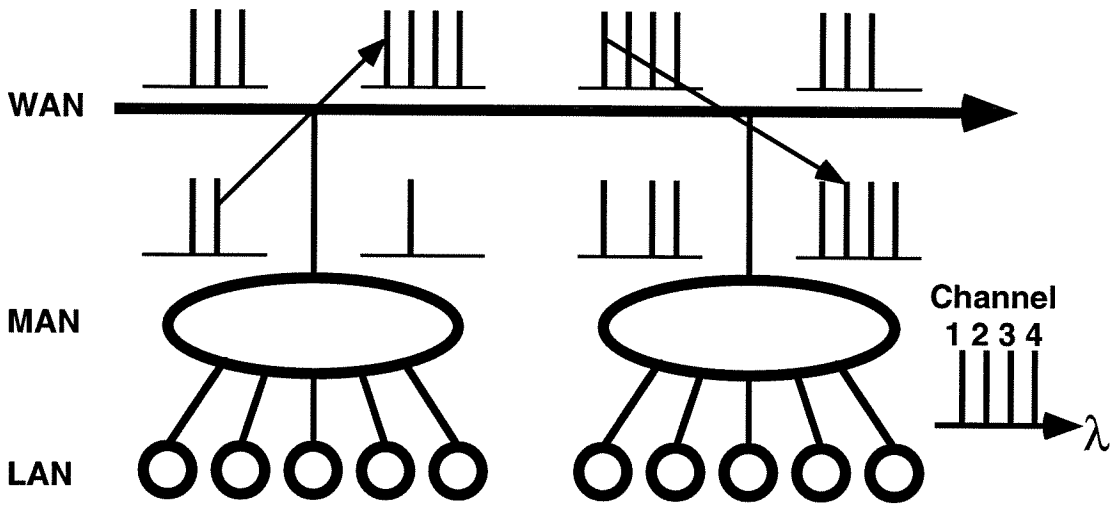

Figure 2.1: A schematic diagram of a possible all-optical network. All interconnections between the various levels are done optically, with wavelength conversion capabilities. Signals on the LANs travel clockwise, while the signals on the WAN travel left to right.

changeable, in order to provide robust, fault tolerant service. And finally, ideally, it should be "transparent" to both bit rate and modulation format, meaning that the converters should be able to handle any bit rate or modulation format, accommodating a large number of services and protocols.

A crucial element for implementation of these complex WDM systems is a wavelength converter [6, 7]. Wavelength conversion in a WDM network could be utilized as shown in Figure 2.1. The signals shown are traveling left to right on the trunk line and clockwise in the MANs. The signal in Channel 3 in the MAN on the left needs to go to the MAN on the right. To do this, first it needs to go onto the trunk

line. Locally Channel 3 is filled on the trunk line, blocking direct routing of the signal from the MAN. A wavelength converter would allow the signal in Channel 3 to be converted to Channel 1 and then to be multiplexed onto the trunk line. Further down the trunk line, it is again blocked from directly moving onto the MAN on the right. Wavelength converting it to the open channel on this MAN allows successful completion of the routing.

Although smaller, simpler networks do not exhibit significant performance improvement from the use of wavelength converters, the larger, more complex networks do as demonstrated in the previous example. A wavelength converter allows efficient frequency reuse between the different interconnected networks. Each of the interconnected networks were able to utilize the same wavelength channels, simplifying mass production of components and supporting scalability of the networks. Converters eliminate wavelength blocking when communicating between levels. Without a converter in the example above, the signal would have been blocked at both of its routing points. Additionally, global knowledge of all the wavelength assignments is no longer necessary, allowing interconnection schedulers to assign wavelengths based on only local information. In the example above, the original router did not need to consider which channels in the destination MAN were open; it simply observed the channel availability locally.

Many technologies exist for the implementation of wavelength conversion [8]. Optoelectronic, cross-gain saturation, and cross-phase saturation wavelength converters are candidate technologies that have been well characterized, however, they are not

transparent to either bit-rate or modulation format. Complete transparency is offered only by ultra-fast wave mixing techniques. Wavelength conversion by FWM has been demonstrated in single-mode fiber [9], semiconductor lasers [10], and semiconductor optical amplifiers (SOAs). In fibers, efficient conversion is achieved only when converting about the zero dispersion point of the fiber. This results in strict limitations, allowing each wavelength to be converted only to one other wavelength for a given converter. Conversion over a limited spectral range has been demonstrated [11], however this required extremely large pump powers. These limitations make FWM in fibers difficult to implement as a wavelength converter for switching between channels in a WDM system. Work on FWM in semiconductor lasers has subsided due to the same problem. The semiconductor laser in which the FWM occurs provides the pump at a fixed wavelength, again limiting the converter to a single wavelength shift for each input. FWM in SOAs is a potential wavelength converter which offers complete transparency to the signal and completely flexible switching.

2.2 Semiconductor Optical Amplifiers

Although recently usurped by Erbium-doped fiber amplifiers (EDFAs) for telecommunications applications in the 1.5 μm band, SOAs were orignally developed for inline optical amplification and for optical preamplification of signals before detection. There is still great interest in them due to their capabiltiy for monolithic integration. Currently, much work is being done using them for novel applications, such as contrast ratio enhancement [12], all-optical demultiplexing [13], packet-header re-

placement [14], all optical WDM-to-TDM conversion [15], all-optical clock recovery [16], and wavelength conversion.

Originally demonstrated in the 1960's [17], an SOA is essentially a semiconductor diode laser biased so that the gain is above transparency but below the lasing threshold. With anti-reflection coatings on the facets of the laser, the lasing threshold is high, allowing for large amplifier gains of over 30 dB. SOAs of InP/InGaAsP can provide gain in the 1.1-1.6 μm band. Amplifiers with active regions comprised of quantum wells provide superior performance over bulk SOAs: higher gain, higher power, greater efficiency, and lower loss. Compressively-strained quantum well SOAs are used for the bulk of the work in this thesis.

In a quantum well SOA, the density of states is given by

$$\rho_{c,v}(E) = \sum_{n=1}^{\infty} \frac{m^*_{c,v}}{\pi\hbar^2} H(E - E_{nc,v}) \quad , \tag{2.1}$$

where c and v correspond to the conduction and valence band, $\hbar$ is Planck's constant, $m^*_{c,v}$ is the effective mass of the carrier in the respective band, and $E_{nc,v}$ is the n^{th} discrete allowable energy level resulting from carrier confinement in the quantum well.

These available states are partially filled by carriers. Under electrical pumping, the probability function describing the filling of the states reaches a quasi-equilibrium described by the Fermi-Dirac law

$$f_{c,v}(E_{c,v}) = \frac{1}{1 + e^{(E_{c,v} - E_{fc,v})/k_B T}} \quad , \tag{2.2}$$

where $E_{c,v}$ and $E_{fc,v}$ are the carrier energy and the quasi-fermi level of the conduction and valence band, k_B is Boltzman's constant, and T is the lattice temperature of the SOA.

The combination of these two functions gives the carrier density and distribution at a quasi-equilibrium point. There are several nonlinear processes which can disturb this equilibrium: spectral hole burning, carrier heating, and carrier density modulation. These are shown in Figure 2.2. Each has a specific mechanism for returning the SOA to equilibrium. It is through modulation of the carrier density and distribution by these nonlinear processes that dynamic gain and index gratings are established and FWM is possible.

Spectral hole burning produces a carrier distribution as shown in Figure 2.2(a). Stimulated emission has burned a hole in the quasi-equilibrium carrier intraband distribution. Carrier-carrier scattering, with a characteristic time constant of 50 - 200 fs, will cause carriers to fill the hole and reach a thermal distribution. However, this results in a Fermi-Dirac distribution that is at a temperature different from that of the lattice of the SOA, as shown in Figure 2.2(b).

Carrier heating produces a similar distribution, either by stimulated emission removing carriers that are cooler than the intraband average or by free carrier absorption exciting carriers to a higher energy level. Carrier-phonon scattering, with a characteristic time constant of 500 - 1000 fs, allows carriers to relax to the lattice temperature. This results in a Fermi-Dirac distribution of the carriers that is at the temperature of the lattice, but that is characterized by a different quasi-Fermi level, as shown in Figure 2.2(c).

Carrier density modulation also produces this distribution, through depletion of the carriers by stimulated recombination. The carrier distribution will return to

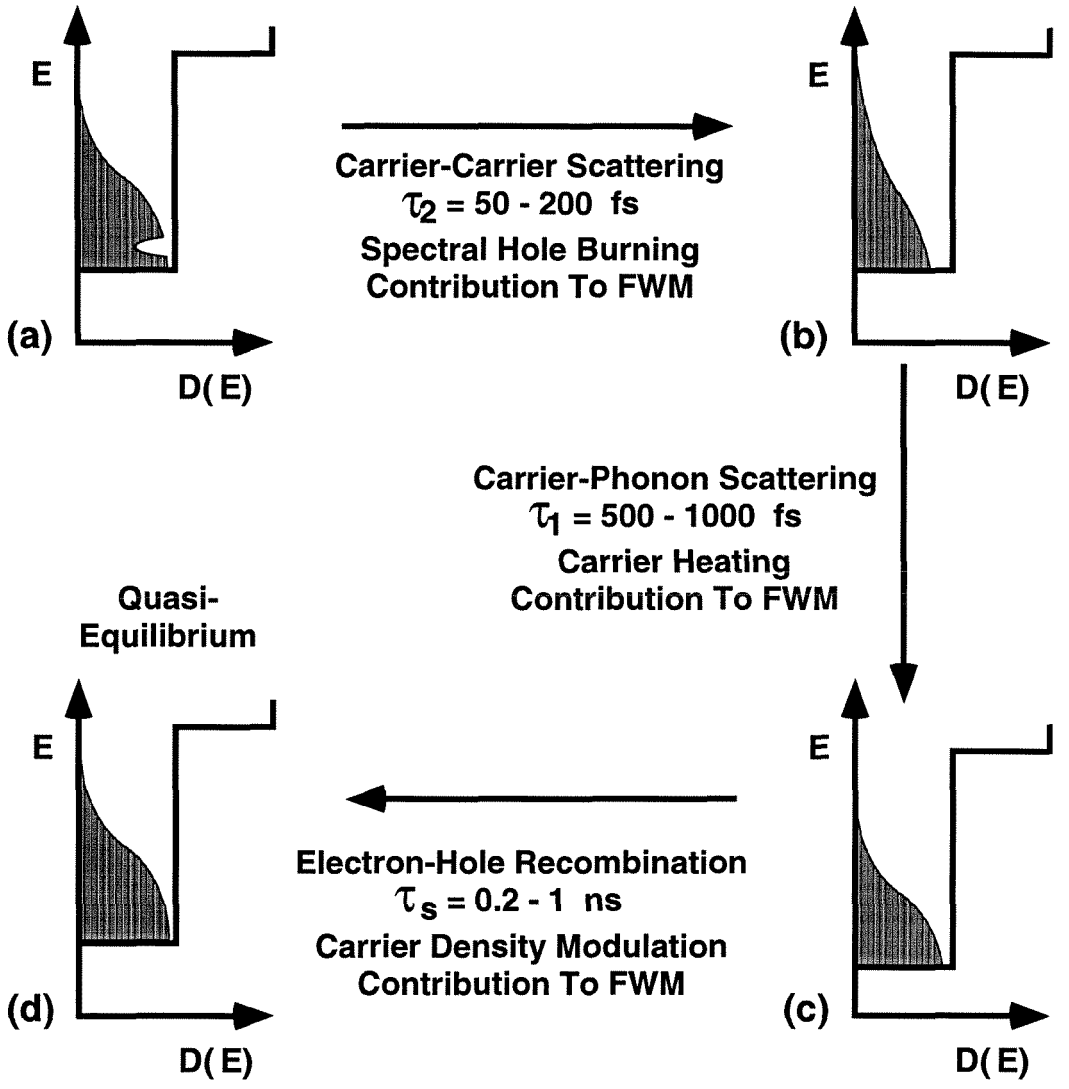

Figure 2.2: Schematic of nonlinear processes contributing to FWM and their effect on the carrier density and distribution. Each plot shows the density of states (line) and the carrier distribution (shaded area).

quasi-equilibrium with a characteristic time equal to the spontaneous emission, 0.2 - 1 ns, as shown in Figure 2.2(d).

Several efforts have measured the time constants associated with the various mechanisms and the strength and phase with which they contribute to the FWM process [18, 19, 20]. Characterizing the conversion efficiency of compressively-strained SOAs, Zhou *et al.* [19] found time constants of 200 ps, 650 fs, and 50 fs and FWM efficiency coefficients of $0.24e^{-1.3i}$, $0.0027e^{1.42i}$, and $0.00023e^{3.13i}$ for carrier density modulation, carrier heating and spectral hole burning, respectively. Hall *et al.* [18] found similar time constants, again for a compressively-strained SOA. Additionally, a delay in carrier heating of 100-200 fs associated with the time for a non-equilibrium distibution to relax to a thermal distribution was shown. This work also characterized the SOA response as a function of the bias current. It found that the spectral hole burning component was almost linearly proportional to the bias current below threshold, approaching zero at threshold.

2.3 Four-Wave Mixing in SOAs

With this fundamental understanding of the nonlinearities in SOAs, it is possible to develop a model to describe the FWM process. The basic principles involved in the process will determine the system limitations of the converter.

Many models of FWM in SOAs have been developed [20, 21, 22]. The work by Mecozzi, [20], is the best model for our specific implementation due to its inclusion of gain saturation. I will present a basic outline of the model and the resulting closed

form solutions. There is, however, a fundamental over-simplification of the gain in this model as it applies to our specific implementation of FWM in SOAs. Unfortunately, taking the gain into account correctly in the model prevents obtaining a closed form solution. After presenting a more accurate gain model for our SOAs, I will then discuss an adaptation of the model to more accurately predict the FWM efficiency of our wavelength conveter.

Figure 2.3 shows a schematic for the experimental configuration we use. Two co-polarized waves are coupled into the SOA. One of the waves, called the pump wave (E_p) with frequency ω_p, is much stronger than the other, called the probe wave (E_q) with frequency ω_q. As implemented in our wavelength converter, the probe wave is the input signal to be converted.

Conceptually, the FWM process can be described as follows. Inside the SOA, the co-propagating, co-polarized pump and probe waves will beat at their detuning frequency, $\Omega = \omega_p - \omega_q$, forming a grating in the electromagnetic field intensity. Through the mechanisms of carrier density modulation, carrier heating and spectral hole burning, dynamic gratings are formed in the SOA carrier density and distribution. The input waves then scatter off of the resulting dynamic gain and index gratings. The pump scattering generates two waves, one at the probe frequency and one at $\omega_{cs} = 2\omega_p - \omega_q$. The probe scattering also generates two waves, one at the pump frequency and one at $\omega_{cs'} = 2\omega_q - \omega_p$. The most interesting of the scattered waves is the converted signal at ω_{cs}. As will be shown, it is more efficiently generated than the other converted wave and, additionally, it is proportional to the phase

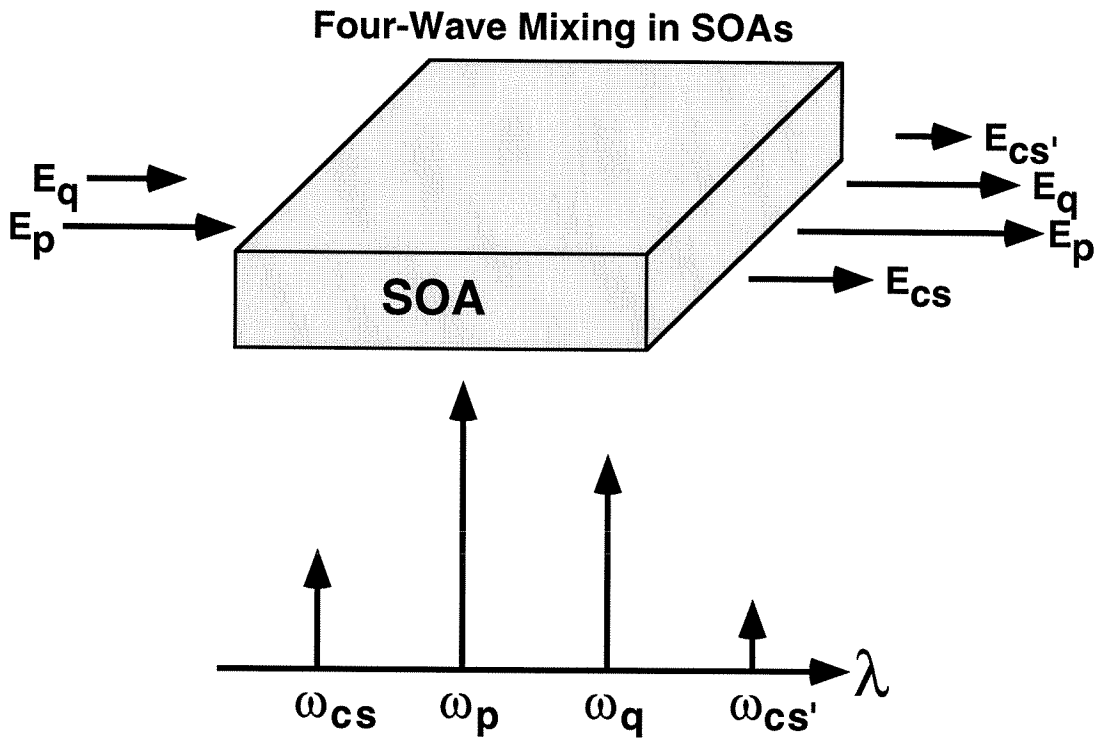

Figure 2.3: A schematic diagram of the experimental configuration used for FWM in SOAs.

conjugate of the input signal.

Modeling the nonlinearities involved in FWM, it is possible to predict the efficiency of the generation of the converted signal. Details of this model can be found in [20, 21]. Beginning with the wave equation for an electromagnetic field

$$\nabla^2 E - \frac{n^2}{c^2}\frac{\partial^2 E}{\partial t^2} = \frac{1}{\epsilon_0 c^2}\frac{\partial^2 P}{\partial t^2} \quad , \tag{2.3}$$

and assuming the form $P = \epsilon_0 \chi(N) E$ for the electric polarization, we can then write

$$\nabla^2 E - \left[\frac{n^2}{c^2} + \frac{\chi(N)}{c^2}\right]\frac{\partial^2 E}{\partial t^2} = 0 \quad . \tag{2.4}$$

Assuming a solution of the form $E(z,t) = E_0(z)e^{i(kz-\omega t)}$, with k_0 defined as the solution for k when $P = 0$, the solution is of the form

$$E(z,t) = E_0(z)e^{i((k_0+knl-i\frac{g}{2})z-\omega t)} \tag{2.5}$$

with

$$g = -\frac{k_0}{n^2}Im[\chi(N)] \tag{2.6}$$

$$k_{nl} = \frac{k_0}{2n^2}Re[\chi(N)] \ . \tag{2.7}$$

Assuming all three waves in the SOA, the pump, the probe and the converted signal, are polarized along the TE mode, the total electric field can be written

$$\begin{aligned} E(z,t) &= E_{pump} + E_{probe} + E_{convertedsignal} \\ &= E_p(z)e^{i(k_pz-\omega_pt)} + E_q(z)e^{i(k_qz-(\omega_p-\Omega)t)} + E_{cs}(z)e^{i(k_{cs}z-(\omega_p-\Omega)t)} \ , \end{aligned} \tag{2.8}$$

where k_i and ω_i are the propagation constant and frequency of the i^{th} wave, respectively. The gain of the TE mode is then assumed to be

$$g = a(N-N_0)\Big[1-\epsilon_{sh}\int_0^\infty dt' h_{sh}(t')|E(t-t')|^2\Big] - g_0\epsilon_{ch}\int_0^\infty dt' h_{ch}(t')|E(t-t')|^2 \tag{2.9}$$

and the nonlinear contribution to the wavenumber is

$$k_{nl} = \frac{1}{2}\Big[\alpha a(N-N_0) - \epsilon_{ch}\beta\int_0^\infty dt' h_{ch}(t')|E(t-t')|^2\Big] \ , \tag{2.10}$$

where a is the gain factor, N is the carrier density, N_0 is the carrier density for transparency, α is the linewidth enhancement factor, g_0 is the normalization gain, β is the linewidth enhancement factor for temperature, $h_{ch}(t)$ and $h_{sh}(t)$ are the response function of the gain to a change in the carrier temperature and in the intraband

population distribution, respectively, and ϵ_{ch} and ϵ_{sh} are the strengths of the carrier heating and spectral hole burning nonlinear processes, respectively. The contributions of carrier heating and spectral hole burning are introduced phenomenologically. The functional dependence follows that measured in [18], with the spectral hole burning response function linear with respect to carrier density below transparency and zero at transparency and with the carrier heating response function non-zero at transparency. There is a small carrier density dependency to carrier heating, however this is neglected.

The carrier density in the SOA is determined by the equation

$$\frac{dN}{dt} = \frac{I}{qV} - \frac{N}{\tau_s} - g|E(z,t)|^2 \ , \tag{2.11}$$

where I is the injection current, q is the charge of an electron, V is the volume of the SOA's active region, and τ_s is the spontaneous lifetime. The carriers will respond to the beating of the pump and the probe, producing a modulation on N at the beat frequency. Assuming a form for N of

$$N = \bar{N} + \Delta N e^{-i\Omega t} + \Delta N^* e^{i\Omega t} \tag{2.12}$$

and using this and Equation 2.8 in Equation 2.11, ignoring terms proportional to ϵ_{ch} and ϵ_{sh}, it is possible to solve for the time-independent terms. One result gives

$$\begin{aligned} a(\bar{N} - n_0) &= \frac{\bar{g}}{1 + \frac{P_t(z)}{P_s}} \\ &= S(z)\bar{g} \ , \end{aligned} \tag{2.13}$$

where $\bar{g} = \frac{aI\tau_s}{qV} - an_0$ is the small signal gain, $P_t(z) = |E_p(z)|^2 + |E_q(z)|^2 + |E_{cs}(z)|^2$ is the total power, $S(z) = \frac{1}{1+\frac{P_t(z)}{P_s}}$ is a saturation parameter whose functional form

is determined by the inital gain function assumed, $a(N - N_0)$, and $P_s = \frac{1}{a\tau_s}$ is the saturation power.

Using these results in the wave equation, under the slowly varying approximation, it is possible to derive the approximate traveling wave equations. Under the assumption $\Omega\tau_s >> 1$, which is true for detunings of interest for a wavelength converter, they can be simplified so as to more easily see the pertinent information.

$$\begin{aligned}
\frac{dE_p}{dz} &= \frac{1}{2}[-\gamma_{sc} + C_1 S(z)]E_p \\
\frac{dE_q}{dz} &= \frac{1}{2}[-\gamma_{sc} + C_1 S(z) - F_1(\Omega)S(z)]E_q \\
\frac{dE_{cs}}{dz} &= \frac{1}{2}[-\gamma_{sc} + C_1 S(z) - F_1(\Omega)S(z)]E_{cs} - \\
&\quad \frac{|E_p|^2 E_q^*}{P_s}[F_2(\Omega) + F_3(\Omega)S(z)] \ , \qquad (2.14)
\end{aligned}$$

where

$$\begin{aligned}
C_1 &= (1 - i\alpha\bar{g}) \\
F_1(\Omega) &= i\Omega\tau_s C_1 \frac{|E_p|^2}{P_s} \\
F_2(\Omega) &= \frac{g_0}{2}\frac{(1 - i\beta)\epsilon_{ch}P_s}{(1 - i\Omega\tau_1)(1 - i\Omega\tau_2)} \\
F_3(\Omega) &= \frac{\bar{g}}{2}\frac{(1 - i\alpha)}{1 + \frac{P_t(z)}{P_s} + i\Omega\tau_s} + \frac{\bar{g}}{2}\frac{\epsilon_{sh}P_s}{(1 - i\Omega\tau_2)} \ , \qquad (2.15)
\end{aligned}$$

and where τ_1 and τ_2 are the time constants associated with carrier heating and spectral hole burning, and γ_{sc} has been introduced phenomenologically to account for waveguide propogation losses. Equation 2.14 shows that the converted signal generated is proportional to the phase conjugate of the input signal, demonstrating the converter's potential as a phase conjugator and also revealing the fundamental modulation format insensitivty of a FWM converter. Additionally, it should be noted

that a similar set of equations could be developed for the FWM converted signal at $\omega_{cs'}$. These equations reveal a reduced conversion efficiency since this converted signal generated is proportional to $|E_q|^2 E_p^*$.

It is possible to obtain a closed form solution from these traveling wave equations, without the simplication of assuming $\Omega\tau_s >> 1$. Solving for the conversion efficiency,

$$\begin{aligned} \eta &= \frac{|E_{cs}(z)|^2}{|E_q(0)|^2} \\ &= \left| \frac{A_{cd}e^{i\phi_{cd}}}{1-i\Omega\tau_s} + \frac{A_{ch}e^{i\phi_{ch}}}{(1-i\omega\tau_1)(1-i\omega\tau_2)} + \frac{A_{sh}e^{i\phi_{sh}}}{1-i\Omega\tau_2} \right|^2 , \end{aligned} \tag{2.16}$$

where the magnitudes and phases of the contributing mechanisms,A_i and ϕ_i for i = carrier density modulation (cd) , carrier heating (ch) and spectral hole burning (sh), are given by

$$\begin{aligned} A_{cd}e^{i\phi_{cd}} &= \left[\frac{P_t(z)}{P_t(0)}\right]^{\frac{1}{2}} \frac{|E_p(0)|^2 ln[\frac{G_0}{G}]}{2P_t(0)}(1-i\alpha) \\ A_{ch}e^{i\phi_{ch}} &= \left[\frac{P_t(z)}{P_t(0)}\right]^{\frac{1}{2}} \frac{|E_p(0)|^2 ln[\frac{G_0}{G}]}{2P_t(0)} \frac{g_0}{g}\left[1+\frac{(G+1)ln[\frac{G_0}{G}]}{2(G-1)}\right](1-i\beta) \\ A_{sh}e^{i\phi_{sh}} &= \left[\frac{P_t(z)}{P_t(0)}\right]^{\frac{1}{2}} \frac{|E_p(0)|^2 ln[\frac{G_0}{G}]}{2P_t(0)} \epsilon_{sh}P_s , \end{aligned} \tag{2.17}$$

where G and G_0 are the facet-to-facet gain and small signal gain, respectively. From this, we can see the functional dependence of the conversion efficiency on the detuning frequency. Each of the three mechanisms has a contributing magnitude and phase, with the magnitude attenuated for increasing detunings by $\frac{1}{1-i\Omega\tau_i}$ as the nonlinearity becomes less able to respond to the higher frequencies. Carrier heating is attenuated by two time constants: τ_1 which corresponds to the carrier-phonon scattering time governing the relaxation of hot carriers, and τ_2 which corresponds to the delay in the turning on of carrier heating.

The measured conversion efficiency as a function of the detuning for our SOA at the operating parameters of our wavelength converter is shown in Figure 2.4. Here we can clearly see the decreased efficiency for increased detunings. Additionally, we can see an asymmetry in the conversion efficiency. Destructive phase interference between the participating mechanisms results in a reduced conversion efficiency for wavelength upshifts.

This model presented is an improvement over Agrawal's model [21] in that it takes into account the gain saturation that occurs in the SOA. This is especially important for our implementation of FWM in SOAs since we operate in the high-input power regime, as discussed in the next chapter, with the SOA heavily saturated. The fundamental over-simplification of this model is that it does not account for gain properly. The assumption of linear dependence of the gain on the carrier density is convenient in that it leads to a closed form solution, however it is incorrect for our SOA, a compressively-strained quantum well device for most of the work presented in this thesis.

As shown by Vahala and Zah [23], the gain of a compressively-strained quantum well SOA can be approximately written

$$g = g_M\left[1 - 2e^{-N/C}\right] \ , \tag{2.18}$$

where g_M is the modal gain and C is a constant taking into account the number of quantum wells. Using this more accurate description of the gain in the carrier density equation, Equation 2.11, it is easily derived that

$$P_t = \frac{C}{g\tau_s} ln\left[\frac{g_M - g}{g_M - g_s}\right], \tag{2.19}$$

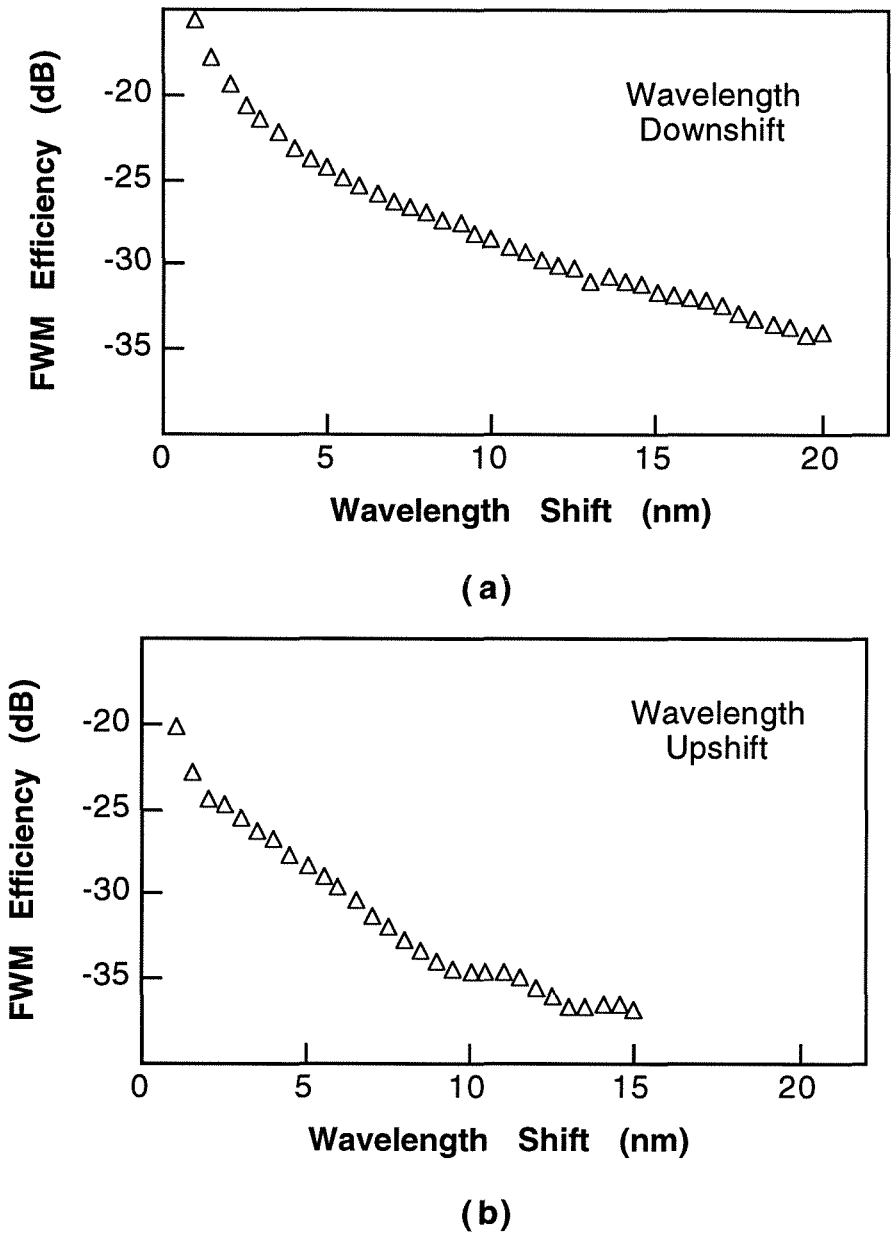

Figure 2.4: Measured conversion efficiency as a function of detunings for shifts both up and down in wavelength

where P_t is the total power in the SOA and g_s is the small signal gain defined as $P \Rightarrow 0$.

Using this functionality for the dependence of the gain, it is impossible to obtain closed form solutions using the framework developed above. However, it is possible to obtain a useful improvement. Using g as defined by Equation 2.19 in Equation 2.14 for $\bar{g}S(z)$, it is possible to correctly determine the facet-to-facet SOA gain as a function of input power for a single input signal through numercial integration. Through proper selection of constants, this model is able to accurately fit the gain measured at the operating parameters of the converter. The functional dependence is approximately equal to

$$\begin{aligned} g &= \frac{g_s}{1+[\frac{P_t(z)}{P_s}]^{1.2}} \\ &= S'(z)g_s \end{aligned} \tag{2.20}$$

for the input power region measured, where $S'(z)$ is a new, more accurate saturation parameter similar to the $S(z)$ in Equation 2.13.

A simple, straight-forward assumption allows incorporation of the more accurate gain model into the traveling wave equations, Equations 2.14, replacing $S(z)$ with the new saturation parameter $S'(z)$ that can accurately fit both the measured gain and the functional dependence of the correct gain model. This provides coupled traveling wave equations which can numerically integrated to predict the conversion efficiency with better accuracy than the simpler model.

2.4 Conclusion

FWM in SOAs is an attractive mechanism for wavelength conversion in all-optical networks. Its conversion efficiency is determined by contributions from three participating nonlinear processes: carrier density modulation, carrier heating, and spectral hole burning. The characteristic time constant associated with carrier density modulation results in reduced contibutions for detunings exceeding 1 GHz, or wavelength conversions of over 0.08 $\mathring{A}$. Carrier heating's and spectral hole burning's contribution remain maximum for detunings of up to 0.25 and 3 THz, respectively, or wavelength shifts of up to 2 and 24 nm. However, the magnitudes of the contributions from the participating processes are approximately inversely proportional to characteristic time constants. Consequently, the conversion efficiency for wavelength shifts of interest in WDM systems (1 - 20 nm) is dominated by contributions from only carrier density modulation and carrier heating.

Bibliography

[1] R. Wagner, "Multiwavelength lightwave networks," *Optical Fiber Communication Conference*, San Diego, California, February 27-March 3, 1995, short course 105.

[2] C.A. Brackett, "Is there an emerging consensus on WDM networking," *J. Light. Tech.*, vol. 14, pp. 936-941, 1996.

[3] R. S. Vodhanel, *et al.* , "National scale WDM networking demonstration by the MONET consortium," *Optical Fiber Communication Conference*, Dallas, Texas, February 16-21, 1997, paper PD27.

[4] B. R. Hemenway, M. L. Stevens, R. A. Barry, C. E. Koskal, and E. A. Swanson, "Demonstration of a re-configurable wavelength-routed network at 1.14 terabits-per-second," *Optical Fiber Communication Conference*, Dallas, Texas, February 16-21, 1997, paper PD26.

[5] R. T. Hofmeister, S. M. Gemelos, C. L. Lu, M. C. Ho, D. Wonglumson, D. T. Mayweather, S. Agrawal, and I. Fishman, "Project LEARN–light exchangeable, add/drop ring network," *Optical Fiber Communication Conference*, Dallas, Texas, February 16-21, 1997, paper PD25.

[6] S.B. Alexander, "A precompetitive consortium on wide-band all-optical networks," *J. Light. Tech.*, vol.11, pp. 714-732, 1993.

[7] C. A. Brackett, "A scalable multiwavelength multihop optical network: A proposal for research on all-optical networks," *J. Light. Tech.*, vol. 11, pp. 736-752, 1996.

[8] S. J. B. Yoo, "Wavelength conversion technologies for WDM network applications," *J. Light. Tech.*, vol. 14, pp. 955-966, 1996.

[9] K. Inoue, "Four-wave mixing in an optical fiber in the zero-dispersion wavelength region," *J. Light. Tech.*, vol. 10, pp. 1553-1561, 1992.

[10] S. Murata, A. Tomita, J. Shimizu, and A. Suzuki, "THz optical-frequency conversion of 1 Gb/s-signals using highly nondegenerate four-wave mixing in an InGaAsP semiconductor laser," *IEEE Photon. Technol. Lett.*, vol. 3, pp. 1021-1023, 1991.

[11] E. A. Swanson, and J. D. Moores, "A fiber frequency shifter with broad Bandwidth, high conversion efficiency, pump and pump ASE cancellation, and rapid tunability for WDM optical networks," *IEEE Photon. Technol. Lett.*, vol. 6, pp. 1341-1443, 1994.

[12] M. Eiselt, "Optical loop mirror with semiconductor laser amplifier," *Electron. Lett.*, vol. 29, pp. 15-17, 1993.

[13] I. Glesk, J. P. Sokolof, and P. R. Prucnal, "Demonstration of all-optical demultiplexing of TDM data at 250 Gb/s," *Electron. Lett.*, vol. 30, pp. 339-341, 1994.

[14] E. Park, D. Norte, and A. E. Wilner, "Simultaneous all-optical packet-header replacement and wavelength shifting for a dynamically-reconfigurable WDM network," *IEEE Phot. Tech. Lett.*, vol. 7, pp. 810-812, 1995.

[15] J. P. R. Lacey, M. V. Chan, R. S. Tucker, A. J. Lowery and M. A. Summerfield, "All-optical WDM to TDM transmultiplexer," *Electron. Lett.*, vol. 30, pp. 1612-1613, 1994.

[16] D. M. Patrick and R. J. Manning, "20 Gbit/s all-optical clock recovery using semiconductor nonlinearity," *Electron. Lett.*, vol. 30, pp. 151-152, 1994.

[17] J. W. Crowe, and R. M. Craig, Jr., "Small-signal amplification in GaAs lasers," *Appl. Phys. Lett.*, vol. 4, pp.57-58, 1964.

[18] K. L. Hall, G. Lenz, E. P. Ippen, U. Koren, and G. Raybon, "Carrier heating and spectral hole burning in strained-layer quantum-well laser amplifiers at 1.5 μm," *Appl. Phys. Lett.*, vol. 61, pp.2512-2514, 1992.

[19] J. Zhou, N. Park, J. W. Dawson, K. J. Vahala, M. A. Newkirk, and B. I. Miller, "Efficiency of broadband four-wave mixing wavelength conversion using semiconductor traveling-wave amplifiers," *IEEE Photon. Technol. Lett.*, vol.6, 50-52, 1994.

[20] A. Mecozzi, S. Scotti, A. D'ottavi, E. Iannone, and P. Spano, "Four-wave mixing in traveling-wave semiconductor amplifiers," *IEEE J. Quantum Electron.*, vol. 31, pp. 689-699, 1995.

[21] G. P. Agrawal,"Population pulsations and nondegenerate four-wave mixing in semiconductor lasers and amplifiers," *J. Opt. Soc. Am. B*, vol. 5, pp. 147-158, 1988.

[22] A. Uskov, J. Mϕrk, and J. Mark, "Wave mixing in semiconductor laser amplifiers due to carrier heating and spectral hole burning," *IEEE J. Quantum Electron.*, vol. 30, pp. 1769-1781, 1994.

[23] K. J. Vahala, and C. Zah, "Effect of doping on the optical gain and the spontaneous noise enhancement factor in quantum well amplifiers and lasers studied by simple analytical expressions," *Appl. Phys. Lett.*, vol. 52, pp.1945-1947, 1988.

Chapter 3

Wavelength Converter Design

3.1 Introduction

When discussing the performance of a wavelength converter, the inevitable figure of merit is its conversion efficiency. Most people abide by the definition: the converted signal power at the SOA output divided by the signal power at the SOA input. However, using this definition, operating at the maximum conversion efficiency point results in a non-optimal optical signal-to-noise ratio (OSNR) at the converter output.

For a systems-level converter, the most important characteristic is its bit-error-rate (BER) performance. However, the simplicity of its design must also be considered. Erbium-doped fiber amplifiers (EDFAs) can give a converter virtually any black-box conversion efficiency, at a sacrifice of the converter's simplicity and performance. For this reason, I feel the appropriate figure of merit for a systems-level converter is a combination of its final OSNR (partially determined by the SOA conversion efficiency) and the simplicity of its design. Although this is somewhat abstract, it is necessary

not to reduce the complicated converter's merit down to a single number: "efficiency".

Based on this, we have optimized the design of our converter by using a high power EDFA and an amplified spontaneous emission (ASE) prefilter. Although this results in reduced conversion efficiency by the standard definition, it offers improved BER performance for an arguably acceptable complication in the converter design. These design aspects are similar to the "optimal converter design", discussed by Zhou [1]. Here the SOA FWM process is broken into two stages: amplification and conversion. With the stages separated by appropriate filters, the optimal OSNR for the converted signal is achieved.

In the following sections, I first present the blackbox design of the wavelength converter. I then further elaborate on operating in the high-input power regime and on the ASE prefiltering technique. The resulting benefits are discussed. Finally, I discuss a potential modification of the converter design to a loop configuration.

3.2 Blackbox Design

A general block diagram for our SOA FWM wavelength converter is shown in Figure 3.1(a). The design is similar, but not identical, to designs presented by other research groups [2, 3, 4]. The converter's pump source is a tunable laser. For the work presented here, we use an external cavity semiconductor diode laser, EOSI Model 2001-ECU. It provides approximately +3 dBm of in-fiber power. With adjustment, it lases single mode over its entire tuning range of 100 nm, from 1480 to 1580 nm.

The pump and probe waves each have individual polarization controllers (PCs)

before being combined. This allows the polarization of the two waves to be aligned to each other and to the proper axis of the SOA. The PCs are the standard paddle-type. Fiber is looped around three paddles of a 2 inch radius, three loops to each paddle. The bending-induced strain in the fiber results in a birefringence approximately equal to a quarter-wave plate for each paddle. The angular position of the three paddles is controlled, effectively allowing independent rotation of three quarter-wave plates. I have heard anecdotal evidence that this does not allow access to the complete set of output polarizations as is claimed. However, in lab we generally align to a linear polarization and are able to obtain minimal loss through a polarizer at the output, so these controllers perform well enough for our purposes.

Once their polarizations are aligned, the input signal and the pump are combined with a standard,tapered-fused fiber bidirectional coupler (BDC). We use one with an 80/20 coupling ratio, giving 80% of the pump and 20% of the input signal in the output fiber. This gives us enough power to fully saturate the subsequent EDFA, and it also gives access to a wide range of pump-to-probe ratios (P/Qs) for input signal powers similar to standard telecommunications power levels (around 0.01 to 1 mW).

The combined signals are then amplified in a high-power EDFA. This allows us to operate in the high-input power regime in the SOA, discussed in the following section. We use an Amoco EDFA, Model 1.5 AMP. It is designed to provide +21 dBm output power. Its performance is slowly degrading, providing an output power of about +19 dBm for most of the experiments presented here.

After amplification, the signals pass through a 10 nm wide bandpass filter (BPF).

We utilize a angle-tuned, interference filter, DiCon Model TF-9-1565-FC/APC-P-L-3. The filter passes both the pump and input signal, with the falling edge of the filter placed on the converted signal side of the pump to suppress the ASE in the spectral region of the converted signal. This filtering is done to increase the OSNR of the converted signal through ASE prefiltering, discussed in a subsequent section.

Following the ASE prefiltering, these signals are coupled into the SOA where FWM generates the converted signal. The SOA is a fiber pigtailed unit from SDL based on a multi quantum-well, compressively strained gain medium with 21 dB fiber-to-fiber small signal gain.

A typical SOA output for this setup is shown in Figure 3.1(b). For the 20 nm shift shown, the pump and the probe are separated by the entire width of the ASE prefilter. The converted signal shows an OSNR of almost 20 dB (into 0.1 nm bandwidth). The unused FWM peak is seen at a wavelength 10 nm higher than the input signal. Additionally, the shape of the ASE prefilter is clearly evident in the shape of the background ASE level.

Following the SOA all three waves, the pump, the probe, and the converted signal, are coupled back into fiber. The pump and the original signal are then suppressed using a 1 nm wide tunable BPF centered on the converted signal. Here we again use an angle-tuned interference filter, DiCon Model TF-1-1565-FC/APC-P-L-3. This suppresses the pump by between 8 and 47 dB and the input signal by between 20 and 50 dB for conversions of 2 to 20 nm. The isolated converted signal, with the original signal and the pump suppressed, is then the wavelength converter output.

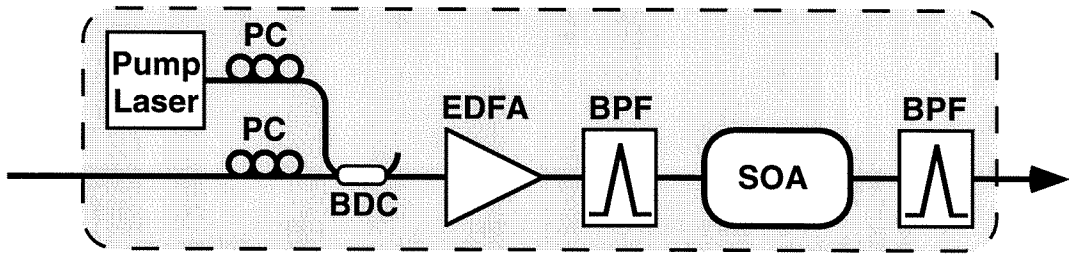

(a)

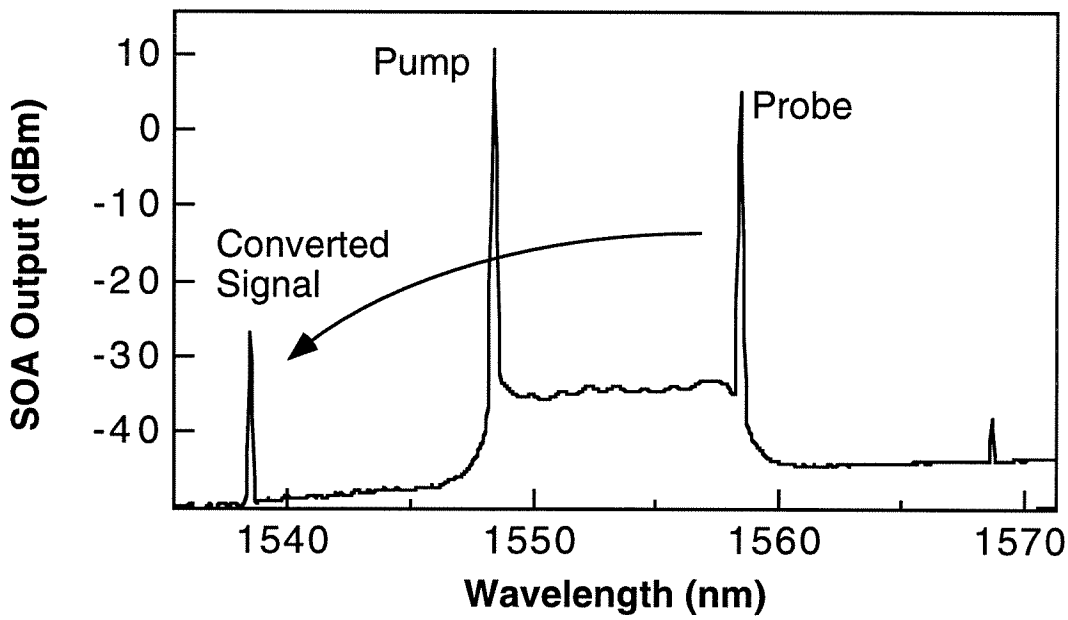

(b)

Figure 3.1: (a) The design of the black box wavelength converter. (b) A typical SOA output, which is filtered in the final BPF to isolate the converted signal before the converter output. Shown are the pump, probe, converted signal, and the additional, unused FWM signal.

3.3 High Input Power Regime

Merely following the formalisms developed by Mecozzi [5], it is possible to predict the conversion efficiency for a given conversion and the resulting OSNR of the converted signal as a function of the total input power. The results show that for a given shift there is a maximum for conversion efficiency, occurring at total input powers of < 0 dBm for a typical SOA. However, as I have previously argued, this is not the optimal operating point. From the same formalisms, one can derive that the converted signal power and the resulting OSNR monotonically increase with increasing total input power.

We measure the standard conversion efficiency of our converter and resulting OSNR versus total input power by inserting a variable attenuator before the SOA, measuring the total input power at the SOA input and the converted signal power at the SOA output. This is done both with and without the ASE prefilter. For all input powers, there is a P/Q of 6 dB and a downshift of 6 nm. The results are shown in Figure 3.2(a). The conversion efficiency is observed to monotonically decrease from -16 to -25 dB for input powers from -5 to 14 dBm.

The OSNR of the converted signal is also shown for the same range of input powers in Figure 3.2(b). Despite the decreasing conversion eficiency, the resulting OSNR is observed to monotincally increase from 5 up to almost 30 dB (with ASE prefiltering) for input powers from -5 to 14 dBm.

Optimizing the wavelength converter performance, we have designed the converter to operate in the high-input power regime. With the degraded performance of our

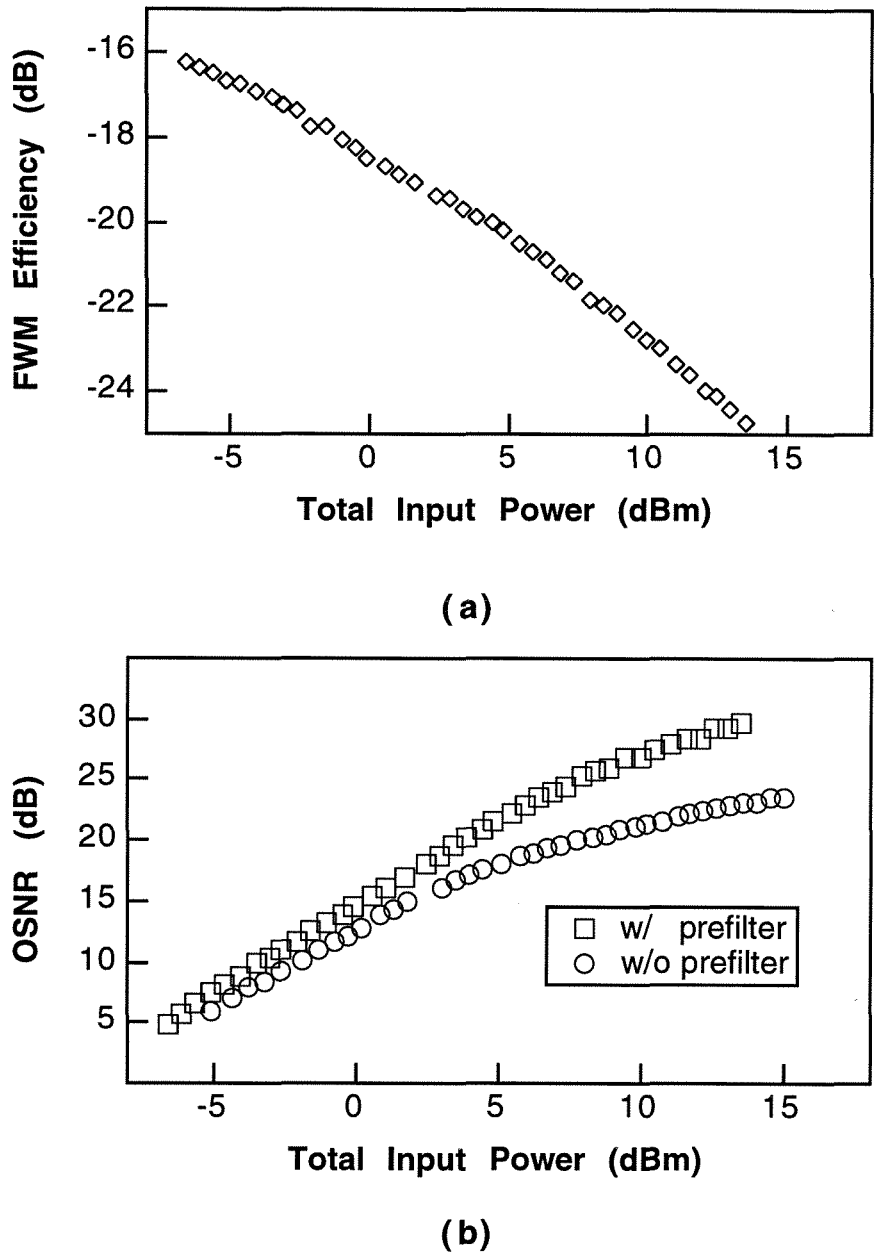

Figure 3.2: Measured dependence of (a) conversion efficiency and (b) OSNR of converted signal (with and without ASE prefilter) as a function total input power.

high-power EDFA, the loss introduced by the ASE prefilter, and the loss intrinsic in coupling the signals from fiber into the SOA, we approximate a total input power of about +12 dBm. This results in a reduced conversion efficiency by the standard definition, however it provides OSNR large enough to demonstrate the wide conversion spectral range presented in the next chapter.

3.4 ASE Prefiltering

Although adding to the complexity of the design of the wavelength converter, the ASE prefilter provides invaluable improvement to its performance. Without it, the background ASE at the SOA output in the spectral region of the converted signal is dominated by the ASE from the high-power EDFA amplified by the SOA, not ASE from the SOA itself. By suppressing the ASE of the high-power EDFA at the converted signal wavelength with the ASE prefilter, the OSNR of the converted signal at the SOA output is increased. This technique of ASE prefiltering between the high-power EDFA and the SOA was first described and demonstrated by Zhou, *et al.* [6], with the tunable BPF first presented by Wilner *et al.* [4].

The improvement in OSNR of the converted signal can be easily seen in the power spectrum at the output of the SOA, as shown in Figure 3.1(b). The background ASE level between the pump and the input signal is dominated by the ASE of the high-power EDFA, amplified by the SOA. Outside of this region the ASE from the power amplifier has been suppressed. Here the background ASE level is dominated by ASE from the SOA itself. It is clearly seen that the ASE prefiltering gives us a

decrease in the background ASE level at the spectral region of the converted signal.

Without the loss introduced by the ASE prefilter, each of the signals at the SOA output would be a 1 to 4 dB higher. However, the background ASE level in the spectral region of the converted signal would then be about 10 dB higher, dominated by the ASE from the high-power EDFA amplified by the SOA. This drastic increase in the background ASE level results in an decrease of the OSNR by 5 to 7 dB, depending on the exact wavelength of the various signals. Figure 3.2(b) shows the 6 dB improvement resulting from ASE prefiltering for a 6 nm shift at high-input powers.

3.5 Loop Filtering

As described in the second section of this chapter, the design of the wavelength converter utilizes two BPFs: one for ASE prefiltering and one to isolate the converted signal at the converter output. These filters are necessary for the converter design used, however they do increase the cost and complexity of the converter. In small quantities they cost $1500-2500 and they require tuning for different wavelength conversions. Additionally, it is arguable that the filters we used might not provide switching speeds quick enough for implementation in actual systems, although other filters untested by us may. There is however a method for implementing wavelength conversion by FWM in SOAs which eliminates the neccessity for these filters.

Originally proposed for fiber converters by Swanson *et al.* [7], with further refinements demonstrated by Mori *et al.* [8], this technique involves mixing in a fiber

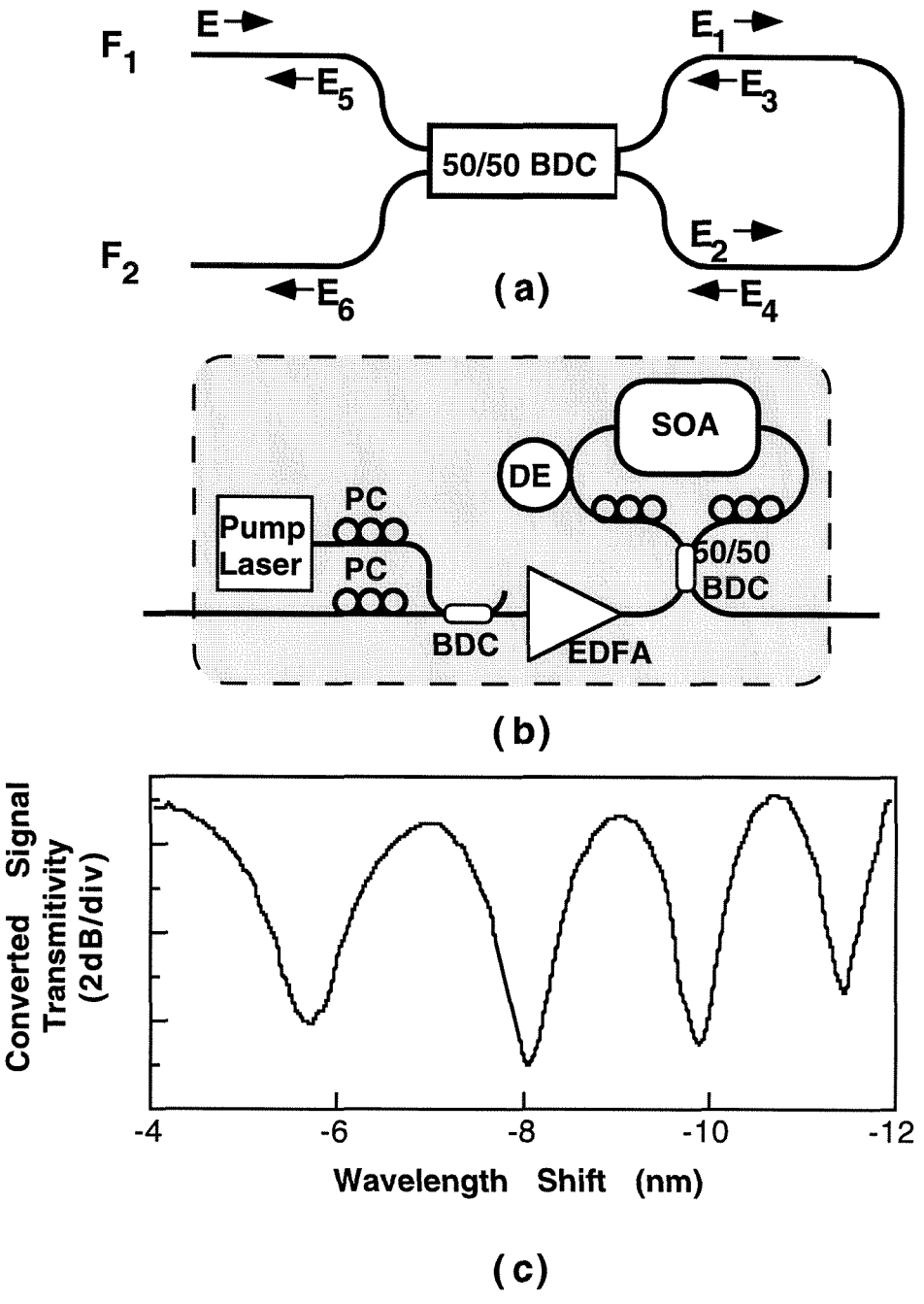

Figure 3.3: (a) Loop reflector (b) FWM Loop Converter (c) Converted signal reflection.

loop reflector [9] for filtering. The principles of a loop reflector are simple, and are not limited to implementation in fiber. Signals are input into a 50/50 BDC in fiber F1 as shown in Figure 3.3(a). The BDC introduces a $\pi/2$ phase shift into the signal coupled over to the other fiber. The two output fibers of the BDC are connected, forming a closed loop. The signals then traverse the same paths, in opposite directions, returning to the BDC. Here both signals are split again and combined in the input fibers of the BDC, traveling in the opposite direction from the input signal. With an input signal of E it is simple to derive, with proper polarization control, that resulting reflected (E_5) and transmitted (E_6) signals are

$$\begin{aligned} E_5 &= \frac{1}{\sqrt{2}}E_3 + e^{I\pi/2}\frac{1}{\sqrt{2}}E_4 \\ &= \frac{1}{\sqrt{2}}e^{I\pi/2}\frac{1}{\sqrt{2}}E + e^{I\pi/2}\frac{1}{\sqrt{2}}\frac{1}{\sqrt{2}}E \\ &= e^{I\pi/2}E \\ E_6 &= \frac{1}{\sqrt{2}}E_4 + e^{I\pi/2}\frac{1}{\sqrt{2}}E_3 \\ &= \frac{1}{\sqrt{2}}\frac{1}{\sqrt{2}}E + e^{I\pi/2}\frac{1}{\sqrt{2}}e^{I\pi/2}\frac{1}{\sqrt{2}}E \\ &= 0 \ . \end{aligned} \tag{3.1}$$

This results in complete reflection of a signal input into the loop reflector.

Swanson *et al.* [7] demonstrated FWM within the loop to eliminate the need for an ASE prefilter. A non-linear element, standard non-dispersion shifted fiber, was inserted in the loop. With the pump and the probe input on fibers F1 and F2, respectively, the converted signal is reflected in fiber F2 with only the probe. The pump and the ASE generated from amplifying the pump are reflected on fiber F1, isolated from the converted signal. For this, the single BPF at the converter output

to suppress the original signal was all that was required. A further modification eliminated the need for this BPF [8].

Introducing a dispersive element (DE) in the loop, to one side of the non-linear element, changes the requirements for total reflection of the converted signal. With the pump and the probe now both input on fiber F1, they are still both completely reflected. However, due to the dispersive element, the converted signals counterpropagating in the loop now have phase difference other than $\pi/2$ when they are split by the BDC and recombined. The phase difference is introduced because traveling in one direction around the loop, the pump and probe waves see the dispersive element before generating the converted signal. Traveling in the other direction around the loop, the converted signal is generated before encountering the dispersive element. With the dispersive element introduced into the loop, the converted signal transmitted in fiber F2 is now

$$E_6 = P_{FWM}\frac{1-\cos\Delta\beta L}{2} \quad , \tag{3.2}$$

where P_{FWM} is the total converted signal power generated by the bidirectional FWM, L is the length of the dispersive element, and $\Delta\beta = \beta_2(\omega_p)[\Delta\omega]^2$ to third order in ω where $\beta_2(\omega_p)$ is the group-velocity dispersion of the dispersive element and $\Delta\omega$ is the detuning frequency $(\omega_{pump} - \omega_{probe})$. In this respect, it is possible to utilize the loop to replace both the ASE prefilter and the BPF at the output of the wavelength converter. With the proper amount of dispersion, corresponding to the proper wavelength shift for a given dispersive element, the converted signal is completely transmitted in the output fiber F2.

We experimentally demonstrated input signal and pump suppression using this technique, utilizing an SOA for the non-linear FWM element for the first time. The converter design is shown in Figure 3.3(b). The dispersive element utilized is 60 m of standard, non-dispersion shifted fiber. Several imperfections limit the performance of this converter with respect to complete reflection of the input signal and pump and complete transmission of the converted signal. Any deviation from an ideal 50/50 BDC, any asymmetry in the fiber-to-SOA coupling between the two sides of the SOA, and any asymmetry in the anti-reflection coatings on the two sides of the SOA prevent the complete reflection or transmission of the signals out of a single port. Utilizing the intra-loop PCs, we are able to compensate for imperfections and maximize the reflection of the pump and input signal. The suppression of the input signal and pump is excellent, with 20 to 30 dB of cancellation in the converter output fiber. This, however, results in incomplete transmission of the converted signal out of the converter output fiber.

Figure 3.3(c) demonstrates the primary limitation of this method, showing the transmission of the converted signal out of the loop wavelength converter (the converted signal power at the converter output divided by the conversion efficiency) as a function of wavelength shift. The proper transmission of the converted signal is achieved only for specific wavelength shifts. Increasing the amount of dispersion in the dispersive element will increase the spectral width of transmission peaks, however it will also move the position of the first peak to a further shift. Still, one could potentially implement a useful converter using this mechanism. Additionally, monolithic

integration of the converter (a potential improvement possible for SOA FWM loop converters but not fiber FWM loop converters) lends itself nicely to this method. It is feasible that the pump source, amplifier, BDC and loop with SOA and dispersive element could all be implemented on a single chip.

Although we did successfully demonstrate input signal and pump suppression, we were unable to perform BER analysis on the converted signal. Primarily, this was due to fluctuations in the transmitted pump power. Due to the large amount of fiber in the loop, with minimal acoustic isolation and no temperature stabilization, the transmittivity of the pump and input signal would fluctuate rapidly by almost 10 dB. This would cause fluctuations in the gain saturation of the EDFA preamplifier in the preamplified receiver, resulting in a garbled detection of the signal. This problem should easily be solvable by monolithic integration of the loop configuration, allowing for easy temperature and acoustic stabilization.

Additionally, there was a problem with the converted signal itself. It appeared as if there was some inter-symbol interference (ISI) occurring from the asymmetry in the loop design. Different counterpropagating bits encounter the SOA at the same time, causing ISI through cross-gain saturation. This problem should also be solvable. Through proper design, with the SOA at the mid-point of the loop, the possibility for ISI should be eliminated as each bit would encounter only its counterpropagating counterpart in the SOA. So although not completely demonstrated yet, a monolithically integrated SOA FWM loop converter should be able to provide a compact wavelength converter with minimal latency.

Bibliography

[1] J. Zhou, "Four-wave mixing in semiconductor optical amplifiers for terahertz spectroscopy and wavelength conversion," Thesis, California Institute of Technology, 1995.

[2] R. Ludwig, and G. Raybon, "BER measurements of frequency converted signals using four-wave mixing in a semiconductor laser amplifier at 1, 2.5, 5, and 10 Gbit/s," *Elec. Lett.*, vol. 30, pp. 338 - 339, 1994.

[3] M. C. Tatham, X. Gu, L.D. Westbrook, G. Sherlock and D.M. Spirit, "Transmission of 10 Gb/s directly modulated DFB signals over 200 km standard fibre using mid-span spectral inversion," *Electron. Lett.*, vol. 30, pp. 1335-1336, 1994.

[4] W. Shieh and A. E. Wilner, "SNR improvement of four-wave mixing wavelength shifting by noise prefiltering in a semiconductor optical amplifier," *Conference on Lasers and Electro-Optics*, Anaheim, California, June 2-7, 1996, paper CThB5.

[5] A. Mecozzi, S. Scotti, A. D'Ottavi, E. Iannone and P. Spano, "Four-wave mixing in traveling-wave semiconductor amplifiers," *IEEE J. Quantum Electron.*, vol. 31, pp. 689 - 699, 1995.

[6] J. Zhou, and K. J. Vahala, "Noise reduction in FWM wavelength converters," *Conference on Lasers and Electro-Optics*, Baltimore, Maryland,May 21-26, 1995, paper CThT1.

[7] E. A. Swanson and J. D. Moores, "A fiber frequency shifter with broad bandwidth, high conversion efficiency, pump and pump ASE cancellation, and rapid tunability for WDM optical networks," *IEEE Photon. Technol. Lett.*, vol. 6, pp. 1341-1343, 1994.

[8] K. Mori, T. Morioka, and M. Saruwatari, "Optical parametric loop mirror," *Optics Lett.*, vol. 20, pp. 1424-1426, 1995.

[9] D. B. Mortimore, "Fiber loop reflectors," *J. Lightwave Tech.*, vol. 6, pp. 1217-1224, 1988.

Chapter 4

Single Channel Conversion

4.1 Spectral Range Characterization

4.1.1 Introduction

Although FWM in SOAs is a promising mechanism for wavelength conversion, there are many parameters which must be characterized and optimized for the converter to be usefully implemented on a systems level. Perhaps most fundamental to the performance of the converter in a WDM system is its spectral range. The converter must be able to convert over a wide wavelength range. Conversion over the entire EDFA gain bandwidth is optimal, however conversion over 10-20 nms is enough both for use with existing filter bandwidths and for WDM channel switching (WDM standards being discussed have channel separations of 0.8 - 1.6 nm [1]).

The versatility in the choice of wavelength shift is one of the attractive features of FWM in SOAs. Large shifts of up to 65 nm have been measured [2]. The limitation imposed in the spectral range is that the efficiency decreases with increased shift

magnitude. This results in a limited spectral range of the converter. As the efficiency drops, both the converted signal's in-fiber power at the SOA output and its OSNR decrease. Individually, or as a combined effect, these can prevent achieving a low BER. Previous demonstrations have achieved 20 nm shifts at 622 Mb/s [3] and 4 nm shifts of 10 Gb/s signals [4].

Ideally, a wavelength converter for a WDM system would be able to access any channel from any of the other channels. Proof of this capability is demonstrated by accessing the entire spectral region covered by the channels from both of the outside channels, upshifting from the lower channel to the upper channel and downshifting from the upper channel to the lower channel. We have characterized the spectral range of the wavelength converter in a 10 Gb/s communications link [5].

4.1.2 Experimental Setup

The experimental setup for the spectral range characterization is shown in Figure 4.1(a). Signal generation, error detection, and eye analysis is done with a 10 Gb/s bit error rate tester (BERT) (Hewlett Packard Model HP71612A) with a microwave transition analyzer (Hewlett Packard Model HP70820A). The optical signal source, the probe, is an Ortel high-speed distributed feedback (DFB) laser whose output is modulated at 10 Gb/s with a non-return-to-zero (NRZ) pseudo-random bit stream (PRBS) by a $LiNbO_3$ Mach-Zehnder external modulator (AT&T Model m2124AA). To compensate for losses in the modulator, it is followed by an EDFA-BPF pair. This signal, with a power of about 0 dBm, is input into the wavelength converter. Following the wavelength converter is a variable attenuator (JDS Fitel Model IA1503-FAL) and

a tap. This allows us to take BER versus received power data. The attenuated signal is then detected by a preamplified receiver. The equipment used in the system surrounding the wavelength converter is discussed in more detail in Appendix A.

4.1.3 Discussion of Results

Beginning with a probe signal at 1558.5 nm, we characterize the converter for downshifts every 2 nm from 2 to 18 nm. We are unable to achieve BER performance $< 10^{-9}$ for downshifts of 20 nm and greater. The spectra of the original signal and the converted signals at the output of the SOA are shown in the upper panel of Figure 4.2. At a 2 nm shift, the converted signal is 17.9 dB down from the original signal at the SOA output. This falls to 31.7 dB down at the 18 nm shift. The background ASE in the spectral region of the converted signals is approximately constant due to the constant total input power for the various shifts. This level rises slightly at the 2 nm shift due to incomplete suppression of the EDFA ASE by the prefilter. The resulting converted signals have OSNRs ranging from 32 to 24.5 dB (into 0.1 nm bandwidth).

BER versus received power data are taken for each shift. The data presented is for PRBS $2^7 - 1$, however the performance shows minimal pattern dependence (< 0.5 dB) for pattern lengths up to PRBS $2^{31} - 1$. The curves for shifts of 2, 10, and 18 nm are shown in Figure 4.1(b). For the 2 nm shift, the pump suppression by the BPF at the converter output is not sufficient to prevent significant degradation to the receiver sensitivity (defined as the received power required for a BER of 10^{-9}). With a single filter at the converter output, there is a received power penalty of about 3 dB compared to the other conversions. Adding a second BPF in series at the converter

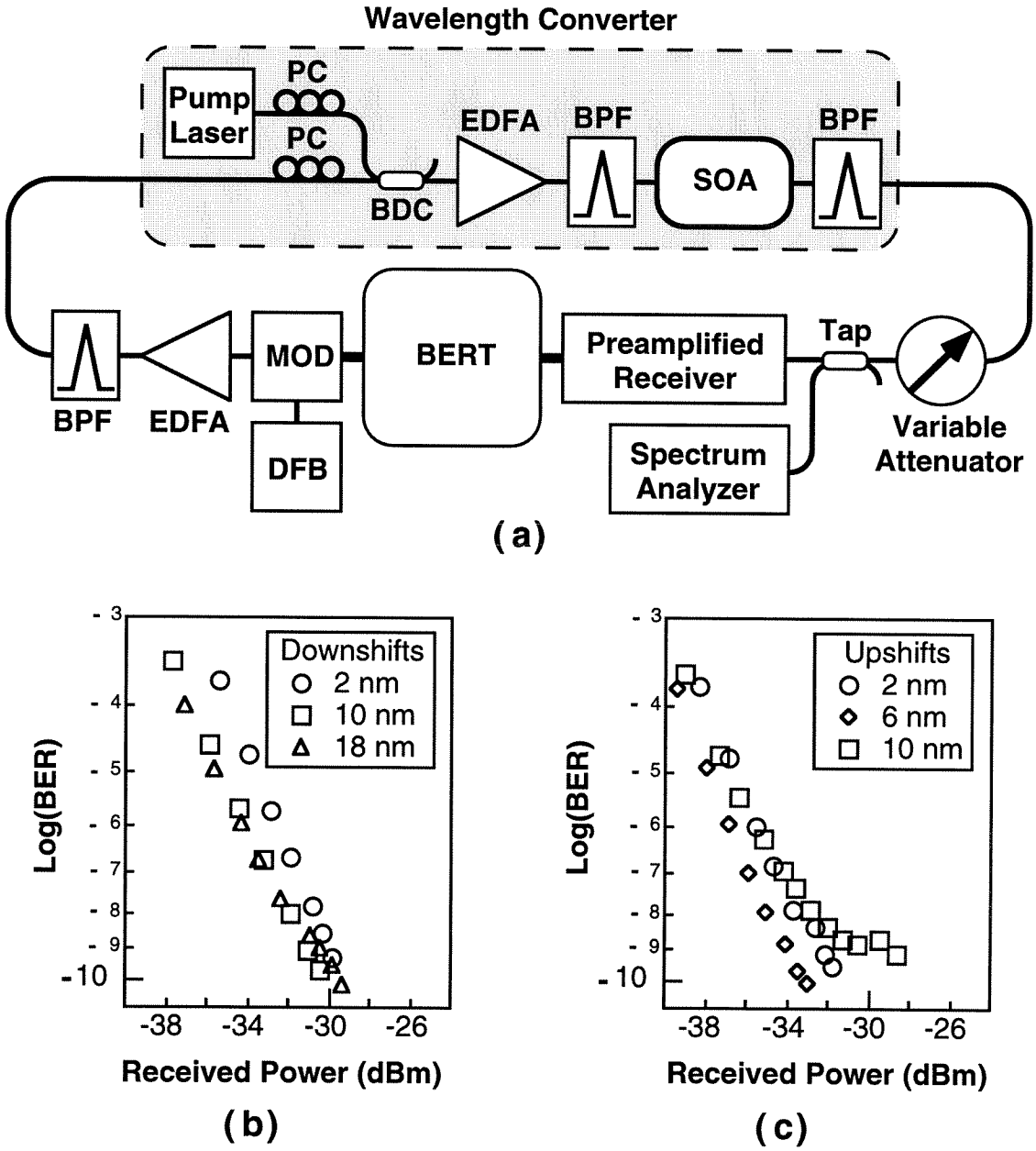

Figure 4.1: (a) The experimental setup for the spectral range characterization. BER performance of the converted signals for selected (b) downshifts and (c) upshifts.

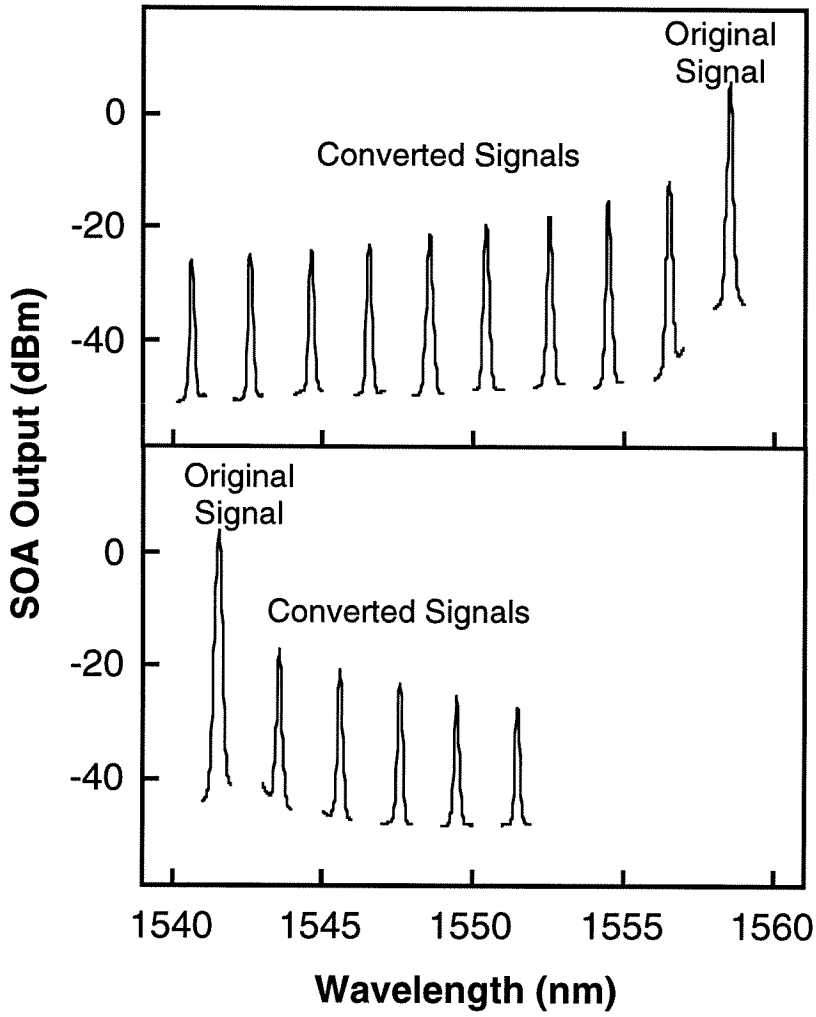

Figure 4.2: The spectra of the converted signals of the complete spectral range of the converter at 10 Gb/s. The converter is able to provide wavelength downshifts of up to 18 nm and wavelength upshifts of up to 10 nm while maintaining a BER performance of better than 10^{-9}

output improves the sensitivity by almost 2 dB, bringing it to within 1 dB of the other curves as is presented. The curve for the 18 nm shift has two features of note. There is a slight flooring at small BER due to the decreased OSNR of the converted signal. Also, BERs $> 10^{-7}$ actually occur at smaller received power then they do for similar BERs of smaller shifts with larger OSNRs. This results from spectral variation in the performance of the receiver, as this converted signal is shifted to a shorter wavelength seeing improved preamplified receiver performance.

Beginning with a probe signal at 1541.5 nm, we characterize the converter performance for upshifts every 2 nm from 2 to 10 nm. We are unable to achieve BER performance $< 10^{-9}$ for upshifts of 12 nm and greater. Original signal and converted signals spectra are shown in the lower panel of Figure 4.2. The reduced efficiency for the upshifts is evident, with the converted signal down 21.0 dB at the SOA outputfor the 2 nm shift and falling to 31.1 dB down for the 10 nm shift. Again, the background ASE is approximately constant, rising slightly for the 2 nm shift. The resulting OSNRs range from 27.1 to 20.5 dB (into 0.1 nm bandwidth). BER versus received power data are again taken for each shift. The curves for shifts of 2, 6, and 10 nm are shown in Figure 4.1(c). The curves display characteristics similar to those for downshifts, with the flooring at low BER for the largest shift much more evident.

In characterizing the capability for shifts both up and down in wavelength, we have effectively demonstrated complete coverage of a 10 nm range by our wavelength converter. Practically, this converter would provide completely flexible switching between any channels of a WDM system with a 10 nm spectral range. Although not

presented here, we have performed a similar experiment with a DFB laser directly modulated at 2.5 Gb/s as the optical signal source. With this input signal, our wavelength converter demonstrated complete coverage of a 16 nm range.

4.2 Dynamic Input Range Characterization

4.2.1 Introduction

For implementation of the converter in a real system, it should ideally be able to accommodate a range of input powers. Random fluctuations of various characteristics of the system, such as temperature, polarization and absolute wavelength, will result in fluctuations of the signal power. The dynamic input range of the converter, or its ability to handle varying input powers, is limited by the dependence of the converter's performance on the P/Q.

The dependence of the dc conversion efficiency on the P/Q is well understood, with a 3 dB ratio being optimal for maximum efficiency. However, it was not previously known if this would be optimal for the case of a modulated input signal. The effect of modulating a high percentage of the power input into the SOA was undetermined; a small P/Q might cause the modulated input signal to disturb the gain saturation of the FWM SOA too drastically and therefore cause inter-symbol interference (ISI). Previously, experiments have simply maintained a large P/Q and mentioned the possibility of this problem [3]. We have experimentally measured the effect of P/Q on the performance of the wavelength converter, characterizing the converter's dynamic input range.

4.2.2 Experimental Setup

To achieve a range of P/Q, the signal's input power to the wavelength converter is varied. This keeps the dc input power to the SOA approximately constant, due to the high level of saturation of the high-power EDFA preceding the SOA. The dc P/Q was varied from 4.7 to 20 dB, with the wavelength shift kept constant at 9 nm. The setup for this experiment is shown in Figure 4.3(a). It is identical to the spectral range experiment except for two areas. First, a variable attenuator is introduced at the wavelength converter input to allow us to vary the input signal power, and consequently the P/Q ratio. Second, the DFB is directly modulated at 2.5 Gb/s by the BERT. This allows us to compare the data with that for the two channel results that will be presented in Chapter 6.

4.2.3 Discussion of Results

BER versus received power data is taken for multiple patterns, PRBS $2^7 - 1$ and PRBS $2^{31} - 1$. The curves for P/Q of 4.7 and 20 dB are shown in Figure 4.3(b). The curves for P/Q = 4.7 show excellent performance, linear with minimal pattern dependence. The curves for P/Q = 20 show degraded performance, with the curves shifted to slightly higher powers and flooring slightly at the small BER. This is due to the reduced OSNR of the converted signal. There is a small pattern dependence to the performance. The longer patterns will have longer strings of "1"s and "0"s, allowing more time for the gain of the SOA to fully saturate and thereby increasing the ISI.

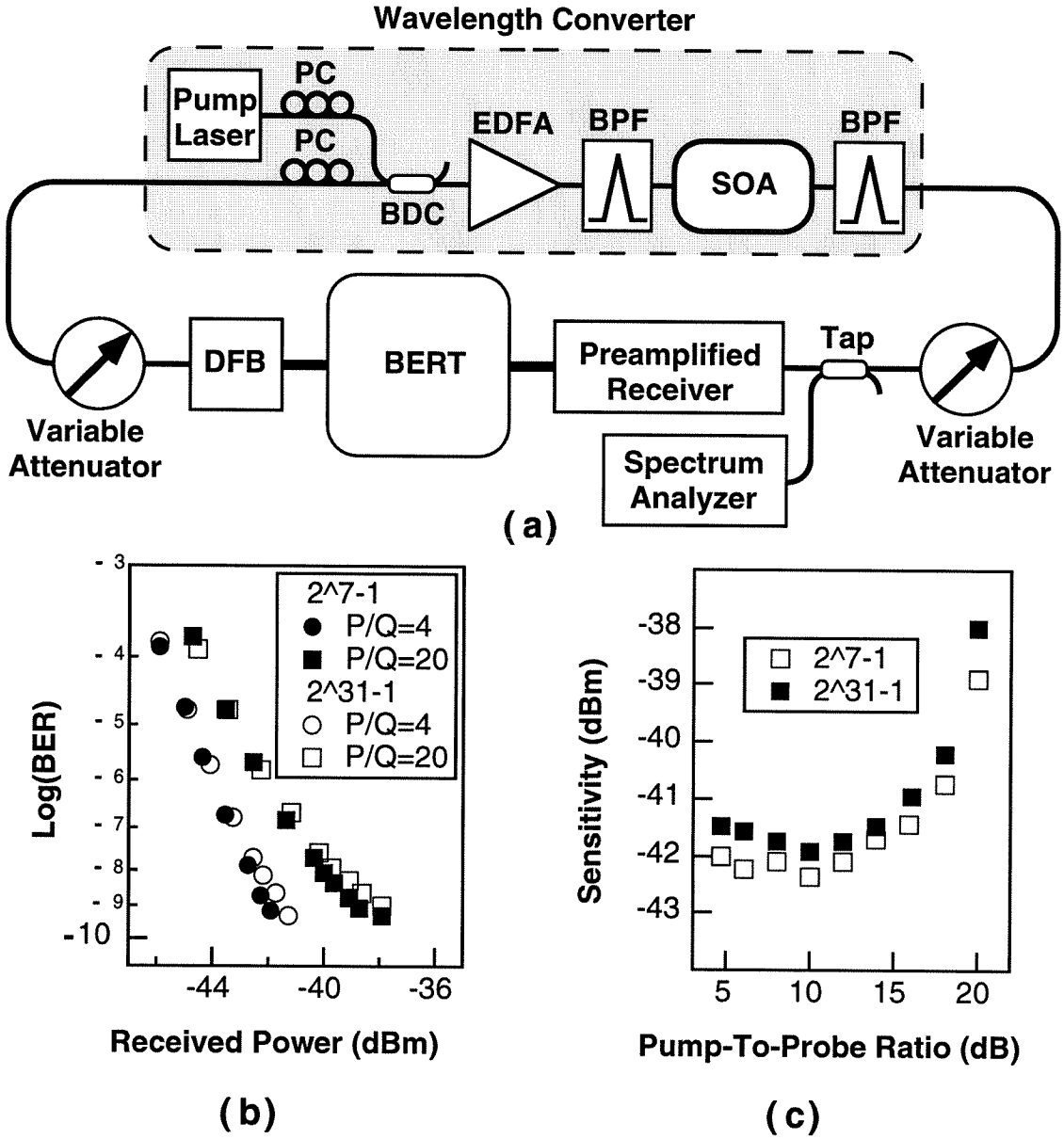

Figure 4.3: (a) Experimental setup to characterize the dynamic input range of the converter. (b) BER performance for two input powers and two pattern lengths. (c) Sensitivity summary of the BER performance for multiple input powers and two patterns.

To further quantify the performance we look at the sensitivity dependence on P/Q. These results are shown in Figure 4.3(c), for P/Q ranging from 4.7 to 20 dB. At a large P/Q, the input signal power is small. This results in a low converted signal power, and consequently a small OSNR at the SOA output. The BER versus received power curves show flooring, causing the sensitivity to be relatively poor. As the P/Q decreases to 10 dB, the converted signal power increases and the OSNR at the SOA output increases. The higher OSNR eliminates the flooring in the curves. As a result, the sensitivity improves.

As the P/Q decreases further, the pump power begins to decrease due to cross-gain saturation between the pump and the input signal in the high-power EDFA and in the SOA itself. This can be easily seen by detecting the pump at the SOA output. The cross-gain saturation introduces an inverted signal on the pump power. It is possible to have BER $< 10^{-9}$ detecting only the pump for P/Q as large as 5 dB. At small P/Q, this cross-gain saturation causes the sensitivity to flatten out due to the reduced pump power and the resulting reduction in conversion efficiency. However, it does so slightly more than would be predicted by a simple model of the gain saturation and conversion efficiency. This may be the effect of additional noise caused by ISI from fluctuations in the saturation of the SOA, but the effect is small and most assuredly not catastrophic.

As seen in Figure 4.3(c), the converter shows relatively flat, consistent performance for P/Qs ranging from about 5 to 15 dB. This shows the wide dynamic range of about 10 dB of acceptable input power of the converter. Additionally, the performance of the

converter is relatively independent of the pattern length, with minimal degradation shown for increasing the pattern length from $2^7 - 1$ to $2^{31} - 1$.

Bibliography

[1] "Wavelength allocation in multiwavelength systems," *Optical Fiber Communication Conference*, Dallas, Texas, February 16-21, 1997, Workshop 205.

[2] J. Zhou, N. Park, K. J. Vahala, M. A. Newkirk, and B. I. Miller, "Four-wave mixing wavelength conversion in semiconductor traveling-wave amplifiers measured to 65 nm of wavelength shift," *IEEE Photon. Technol. Lett.*, vol. 6, pp. 984 - 987, 1994.

[3] M. C. Tatham, G. Sherlock, and L. D. Westbrook, "20 nm wavelength conversion using nondegenerate four-wave mixing," *IEEE Photon. Technol. Lett.*, vol. 5, pp. 1303 - 1306, 1993.

[4] R. Ludwig, and G. Raybon, "BER measurements of frequency converted signals using four-wave mixing in a semiconductor laser amplifier at 1, 2.5, 5, and 10 Gbit/s," *Elec. Lett.*, vol. 30, pp. 338 - 339, 1994.

[5] D. F. Geraghty, R. B. Lee, K. J. Vahala, M. Verdiell, M. Ziari, and A. Mathur, "Wavelength conversion up to 18 nm at 10 Gb/s by four-wave mixing in a semiconductor optical amplifier," *IEEE Phot. Tech. Lett.*, vol. 9, pp. 452-454, 1997.

Chapter 5

Critical Issues For Real System Implementation

5.1 Cascadability

5.1.1 Introduction

With SOA FWM wavelength converters as the interconnection elements between levels in a WDM system, a signal traveling between multiple levels would be required to undergo multiple wavelength conversions. This was demonstrated in the simple scenario given in Chapter 2. Consequently, implementation of converters in scalable WDM networks would require the converters to be cascadable. Cascaded wavelength conversions have been demonstrated at data rates up to 10 Gb/s by cross-gain saturation in semiconductor optical amplifiers (SOAs) [1] and semiconductor lasers [2] and by cross-phase saturation in SOAs [3]. We have performed the first demonstration of

cascaded FWM SOA wavelength converters, and developed a model predicting their ultimate cascadability limits [4, 5].

5.1.2 Experimental Demonstration

We perform an experimental characterization of the degradation to 10 Gb/s signals that results from cascading two SOA FWM wavelength converters providing shifts of equal magnitude. Due to the spectral dependence of the EDFA preamplifier used in the receiver, in order to be able to accurately determine the signal degradation we are required to alternate the direction of the wavelength shift, producing a cascaded-converted signal that has the same wavelength as the original signal.

The system used to characterize the cascaded converters is shown in Figure 5.1(a). The first converter shifts the signal down in wavelength, with the second converter shifting the signal back up to the original wavelength. We characterize the signal performance at various points in the system. First, we look at the original, unconverted signal at the modulator output. Next we characterize the signal after undergoing a single wavelength downshift. Finally we analyze the cascaded converted signal at the output of the second converter both with and without a 40 km section of fiber, followed by an EDFA-BPF pair to compensate for propagation losses, separating the two converters.

The BER performance of the signals for cascaded 5 nm shifts is shown in Figure 5.1(b). The solid line is the baseline, unconverted signal performance. After a single conversion, the signal performance has improved. This is due to the fact that this converted signal sees better performance from the preamplified receiver and that

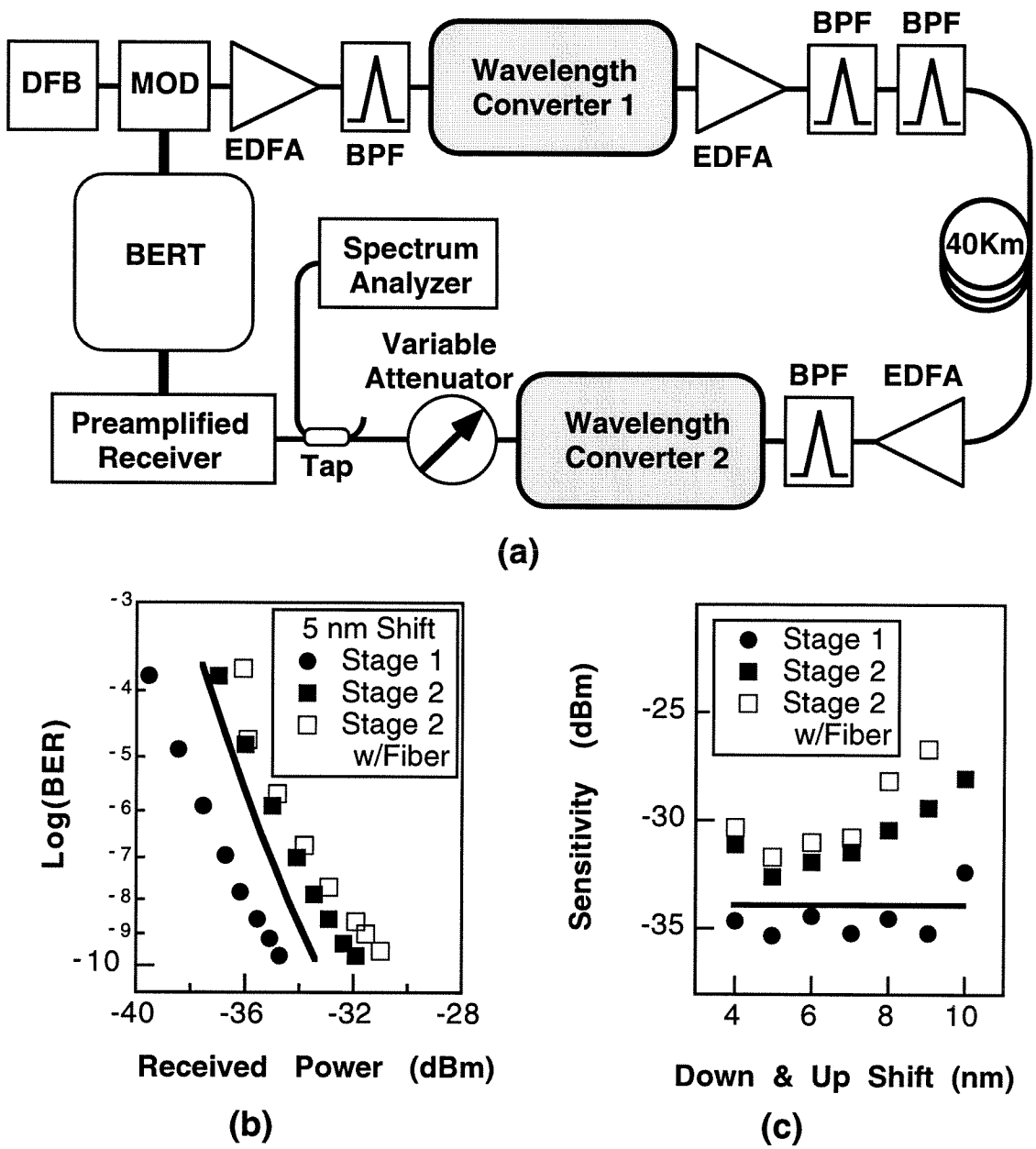

Figure 5.1: (a) Experimental demonstration of cascaded wavelength converters. The cascaded converters are separated by 40 km of standard, non-dispersion shifted fiber to more accurately simulate a real system. (b) BER performance of cascaded 5 nm shifts. (c) Sensitivity summary of the BER performance of the cascaded converters

the dc bias of the modulator is chosen optimizing the performance of the cascaded converted signal. The cascaded converted signal shows minimal degradation to the original signal. The sensitivity (the received power required for a BER of 10^{-9}) has increased by 1.3 dB. The addition of the 40 km fiber section introduces a minimal further degradation of less than 1 dB, resulting primarily from the additional EDFA required.

The sensitivity of the converted signals for cascaded shifts from 4 to 10 nm is shown in Figure 5.1(c). The cascaded 10 nm conversion has a relatively poor sensitivity due to the small OSNR resulting from the 10 nm upshift. As the magnitude of the cascaded shifts decreases, the resulting OSNR increases and the sensitivity of the converted signal improves. It degrades again for the 4 nm shift, however, due to the residual pump from the first converter causing noise in the second converter through an interferometric effect. Better BPFs or non-identical pump wavelengths would eliminate this degradation.

5.1.3 Predicted Limits

Experimentally, we are limited to demonstrating two cascaded FWM SOA wavelength converters, merely by the equipment available. However, using the conversion efficiencies measured in the characterization of the spectral range of the converter, shown in Figure 4.2, we are able to model the limits of the cascadability of this converter. In the model, each converter is followed by an EDFA in order to boost the power of the converted signal to a level high enough to be input into the subsequent converter. The amplified converted signal is then attenuated to +3 dBm. This is the correct

input power for a P/Q of 6 dB for our wavelength converter design, matching the P/Q used in measuring the conversion efficiencies.

A few simple approximations are made to facilitate the model. The background ASE level generated by the SOA is assumed to be constant, independent of the shift. Additionally, the performance of the EDFAs is assumed to be spectrally independent. The constant background ASE level is a reasonable assumption due to the high power level at the SOA input. The wavelength independent EDFA performance is a less reasonable assumption, however it is necessary since the model is general, with no beginning and ending wavelength specified. The background ASE level and the EDFA performance assumed, -49.25 dBm into 0.1 nm bandwidth and 33 dB gain with 4.5 dB noise figure respectively, are set by the performance of our equipment measured at a particular wavelength.

With the large side-mode suppression provided by DFB lasers, the degradation of the OSNR in the first converter results in an output OSNR that is dominated by the ASE from the SOA. At the output of the first converter, the OSNR is approximately

$$OSNR(1) = \frac{P_{FWM}(1)}{N_{SOA}} \quad , \tag{5.1}$$

where $P_{FWM}(1)$ is the converted signal power for the desired shift of the first stage and N_{SOA} is the SOA background ASE level (-49.25 dBm) in watts.

From the definition of the noise figure, it is easily derived that the noise at the output of an EDFA is approximately [6]

$$N_{out} = NF\ h\ \nu\ G\ B_w + G\ N_{in} \quad , \tag{5.2}$$

where NF is the noise figure, h is Planck's constant, ν is the frequency of the converted

signal, G is the gain of the EDFA (assumed to be 33 dB), B_w is the resolution bandwidth, and N_{in} is the input noise. The value of ν was approximated as constant for all of the converted signals wavelengths.

Using this, the OSNR at the output of the i^{th} converter can be written

$$\begin{aligned} OSNR(i) &= \frac{P_{FWM}(i)}{N_{ic}} \\ &= \frac{P_{FWM}(i)}{\frac{P_{FWM}(i)}{OSNR_a(i-1)} + N_{SOA}} \\ &= \frac{P_{FWM}(i)}{\frac{P_{FWM}(i)}{\frac{G\,P_{FWM}(i-1)}{NF\,h\,\nu\,G\,B_w + G\,N_{(i-1)c}}} + N_{SOA}} \\ &= \frac{P_{FWM}(i)}{\frac{P_{FWM}(i)}{\frac{G\,P_{FWM}(i-1)}{NF\,h\,\nu\,G\,B_w + G\,\frac{P_{FWM}(i-1)}{OSNR(i-1)}}} + N_{SOA}}, \end{aligned} \tag{5.3}$$

where $P_{FWM}(j)$ is the converted signal power for the desired shift of the j^{th} converter, N_{jc} is the noise power at the output of the j^{th} converter, and $OSNR_a(j)$ is the OSNR at the output of the EDFA amplifier following the j^{th} converter.

Using these equations, the OSNR is recursively calculated until the resulting OSNR falls below 20.5 dB. This is the OSNR required for 10^{-9} BER detection of a signal that has undergone a single conversion. This defines the cascadability limit of the wavelength converter. It should be noted that this model does not take into account any additional BER performance degradation that may occur from signal distortion or extinction ratio degradation.

The predicted cascadability of our converter is shown in Figure 5.2(a). The number of cascaded shifts possible is calculated for shifts of equal magnitude down and up in wavelength. Up to 37 downshifts of 2 nm are possible. This rapidly drops to only 3 downshifts of 10 nm, with the 18 nm downshift not cascadable. The reduced

conversion efficiency for wavelength upshifts results in reduced cascadability for repeated upshifts. Only up to 11 upshifts of 2 nm are possible, and the converter is not cascadable for upshifts of 8 nm and greater. Alternating between shifts up and down in wavelength provides intermediate cascadability performance, indicated by the shaded region.

An interesting result of this model is that it is possible to get better performance by cascading shorter shifts than by doing a single large shift. Figure 5.2(b) compares the OSNRs resulting from cascaded 2 nm downshifts with those resulting from single larger downshifts. The decreasing conversion efficiency for the larger shifts leads to increasing improvements from cascaded smaller shifts. The reduced efficiency of a large 18 nm downshift gives an OSNR that is over 3.5 dB worse than the OSNR resulting from 9 cascaded 2 nm downshifts.

Possibly the most useful result of this model is to be able to predict the improvement in the cascadability of wavelength converters resulting from improved conversion efficiency. Increased efficiencies could result from improvements in the SOA design, such as saturation power and length. Figure 5.2(c) compares the cascadability for repeated downshifts for our converter with the cascadability for converters with SOAs providing conversion efficiencies 3 and 10 dB greater. The number of cascaded shifts possible is almost directly proportional to conversion efficiency.

It should also be noted that improved EDFA noise figure performance would also increase the cascadability of the converters, with more drastic improvements resulting for cascaded small shifts where more of the OSNR degradation results from the

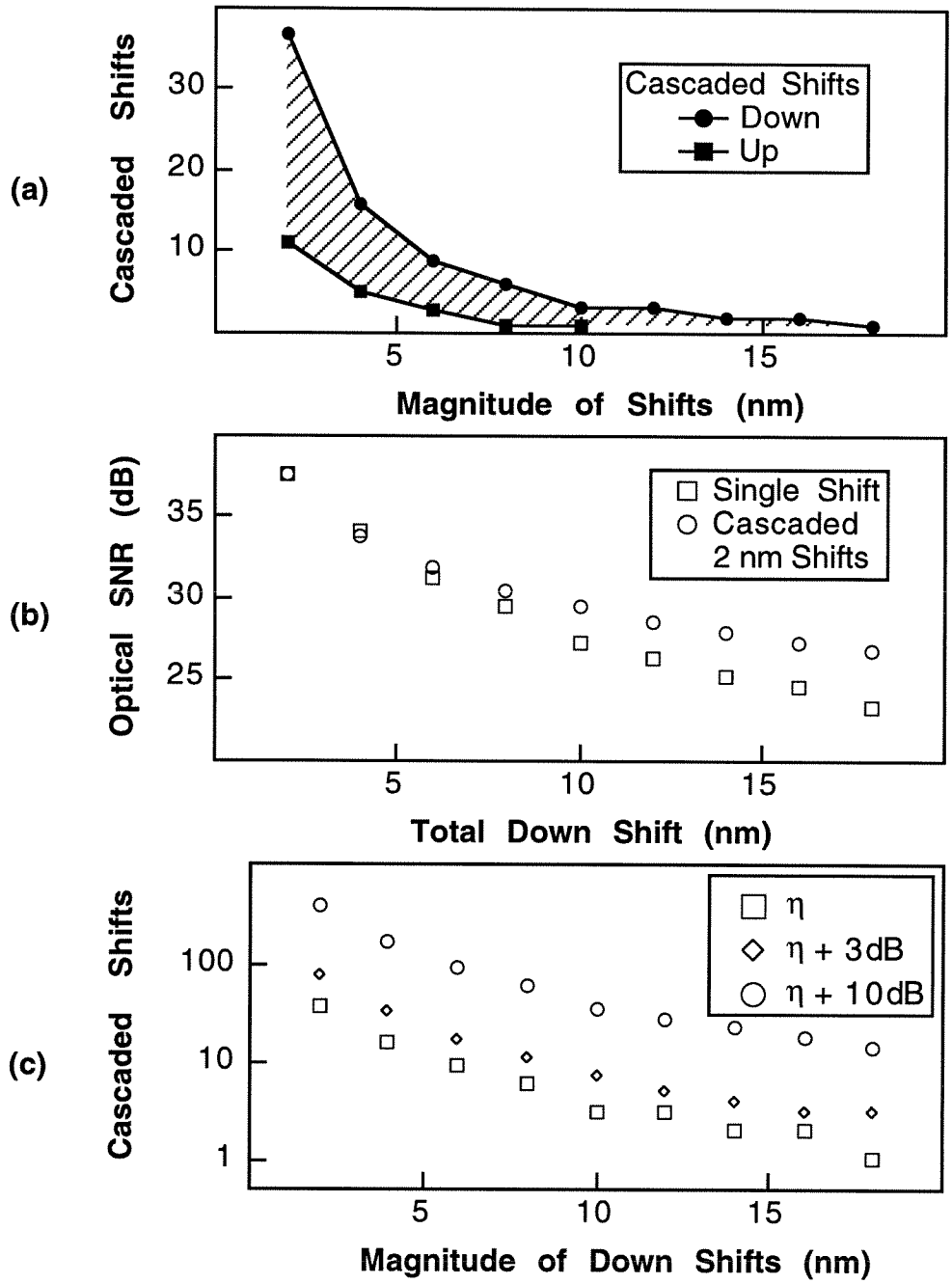

Figure 5.2: Predicted cascadability limits of the converter. (a) Predicted limits of cascaded shifts monotonically down, up and varying in wavelength. (b) Comparison of cascaded 2 nm downshifts and single large downshifts (c) Predicted cascadability improvements resulting from conversion efficiency improvements.

amplification. We have assumed a noise figure of 4.5 dB, well above the theoretically optimal 3 dB.

We have demonstrated cascaded wavelength conversions of up to 10 nm at 10 Gb/s. Additionally, we have predicted the cascadability limits of the converter. The current performance of the converter is potentially suitable for use in an AON. It is defintiely suitable for applications such as signal processing, where multiple small shifts are required. Additionally, we have shown that improved conversion efficiency will result in large improvements in cascadability, making the converter more realistically implementable in an AON.

5.2 Polarization Insensitive Converter Performance

5.2.1 Introduction

Almost all of the fiber in use today in telecommunications systems is not polarization maintaining. For this reason, implementation of wavelength converters will most likely require them to be polarization independent in their performance. A straight-forward, brute-force method is to split the input polarizations, convert each polarization separately, and then recombine them. This, however, is both complicated and expensive, as tandem, single polarization converters are required at each stage. Polarization independent wavelength conversion has been demonstrated by multiple groups [7, 8]

The previous results presented here have used a single pump configuration, due to its simplicity and superior conversion efficiency. As discussed in Chapter 3, the

pump and input signal polarizations in these wavelength converters are aligned with mechanical PCs before being coupled into the SOA. Unfortunately, there is in general no single pump polarization setting which will allow polarization independent FWM wavelength conversion in SOAs. Nearly polarization independent conversion can be obtained by a dual-pump configuration. Limitations imposed are that the wavelength difference between the pumps must be much smaller than the detuning between the pumps and the probe, that the two non-zero off-diagonal components of the susceptibility tensor of the SOA must be nearly equal, and finally that the SOA have polarization independent gain [9, 10, 11].

5.2.2 Mechanisms for Polarization Insensitivity

The polarization states of the two pump lasers are fixed so that one pump is aligned to the TE axis of the SOA and the other is aligned to the TM axis. As shown in Figure 5.3(a), the probe beats with the two pumps to create two gratings in the electromagnetic field intensity: one in the TE polarization and another of a different frequency in the TM polarization, called the slow and fast gratings, respectively. The relative magnitude of these two beat waves is dependent upon the polarization of the input signal relative to the pumps' polarizations.

Through the mechanisms discussed in Chapter 2, these beat waves generate gratings in the carrier density and distribution. The different pump wavelengths result in the two gratings in the tensile well having different frequencies. This prevents them from destructively interfering with each other as the input signal's polarization rotates, changing their phases relative to each other.

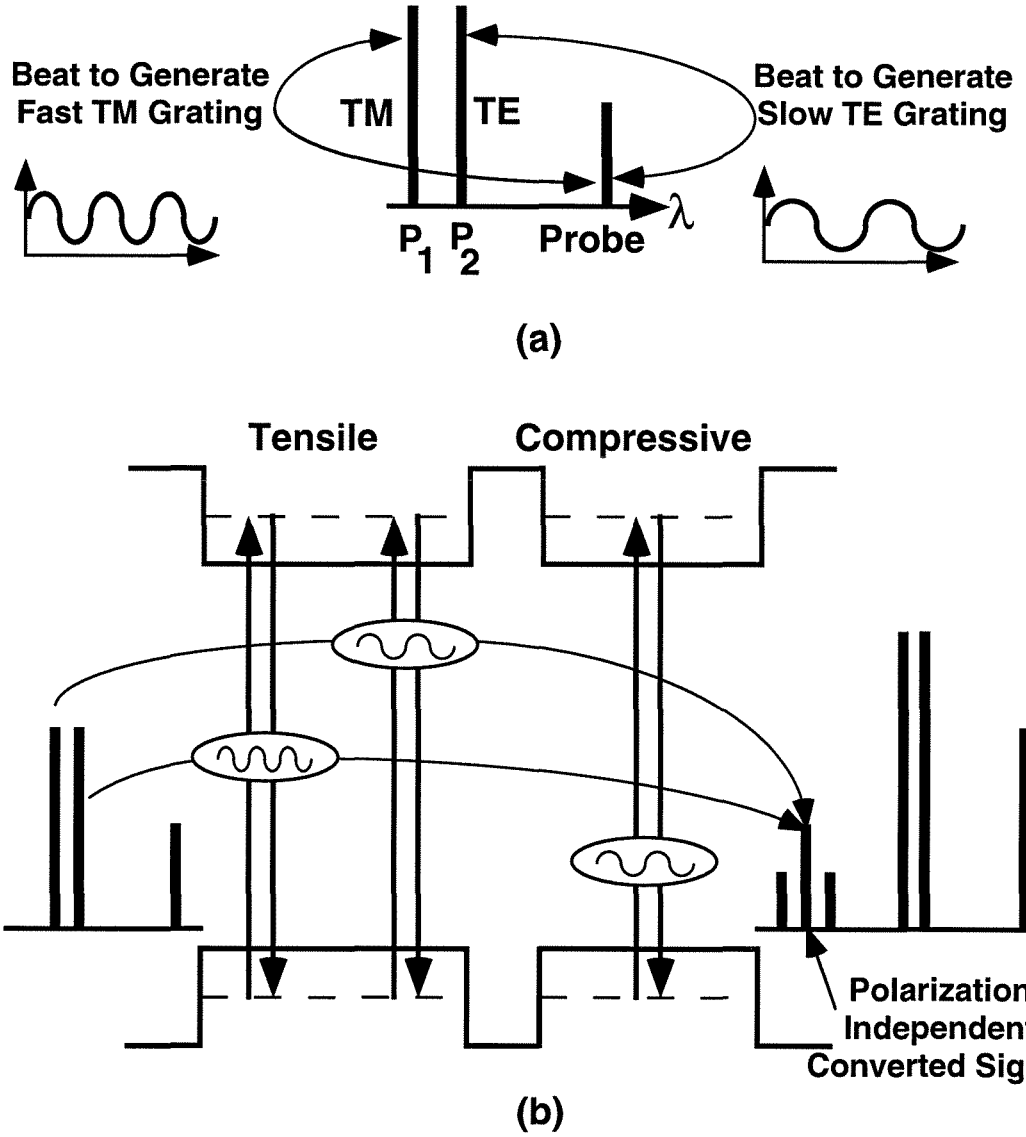

Figure 5.3: Mechanisms for polarization independent wavelength conversion

Each input pump wave then scatters off of the grating established by the beating of the other pump and the probe in the tensile well as shown in Figure 5.3(b). These two scattered waves are at the same frequency, and they add together to generate a polarization independent converted signal. Although not used in the initial generation of the polarization independent wave, the presence of the compressive well is required in order to provide polarization independent gain for this wave once it is generated.

In addition to the desired mixing that occurs, there is mixing identical to the standard FWM configuration. Each pump scatters off of the grating established by its beating with the probe. This generates two polarization dependent single pump wavelength converted signals that arise separated from the polarization independent converted signal by the detuning between the two pumps. These two wavelength converted signals are distinctly polarization sensitive, as their generation requires parallel alignment of the pump and probe waves.

5.2.3 Experimental Setup

The configuration for the dual-pump wavelength converter is shown in Figure 5.4(a). It is identical to the converter presented in Chapter 3 except for two areas. There are 2 pump lasers, each with individual polarization controllers. These lasers are combined with a 50/50 BDC and then amplified and passed through a BPF before being combined with the input signal. The two pumps are an external cavity laser and an Erbium-doped fiber ring laser [12] , separated in wavelength by 0.2 nm. Additionally, there is no PC on the input arm of the converter. The converter's performance should be polarization independent, so the input signal's polarization is no longer controlled.

This converter is characterized in the system shown in Figure 5.4(a). The input signal is a DFB directly modulated at 2.5 Gb/s NRZ PRBS. The polarization of the input signal is controlled external to the wavelength converter to give a range of input polarizations, measured at the input to the SOA. The wavelength of the input signal is set to produce a shift of 6 nm. The detection of the signal is identical to that described in Chapter 4.

5.2.4 Discussion of Results

The inset in Figure 5.4(b) shows a typical output spectrum of the SOA. The signals labeled 1 and 3 are the standard, polarization dependent FWM signals generated by the TM wave and TE wave, respectively. The signal labeled 2 is the polarization independent signal. Also shown are the input signal and the two pumps. Figure 5.4(b) shows the polarization dependence of the 3 converted signals. Here the polarization of the input signal is measured at the SOA input, but the dependence of the converter performance on the polarization of the signal at the converter input will be functionally identical.

Signal 1 is maximum for an input polarization of 0 degrees, when the input signal is aligned to the TM pump. It drops off rapidly as the polarization of the input signal is rotated towards orthogonal to the TM pump. This dependence would be typical of the polarization dependence of the standard, single pump FWM converter performance. Signal 3 demonstrates an opposite polarization sensitivity. It is maximum when the input polarization is orthogonal to the TM pump, when it is aligned with the TE pump.

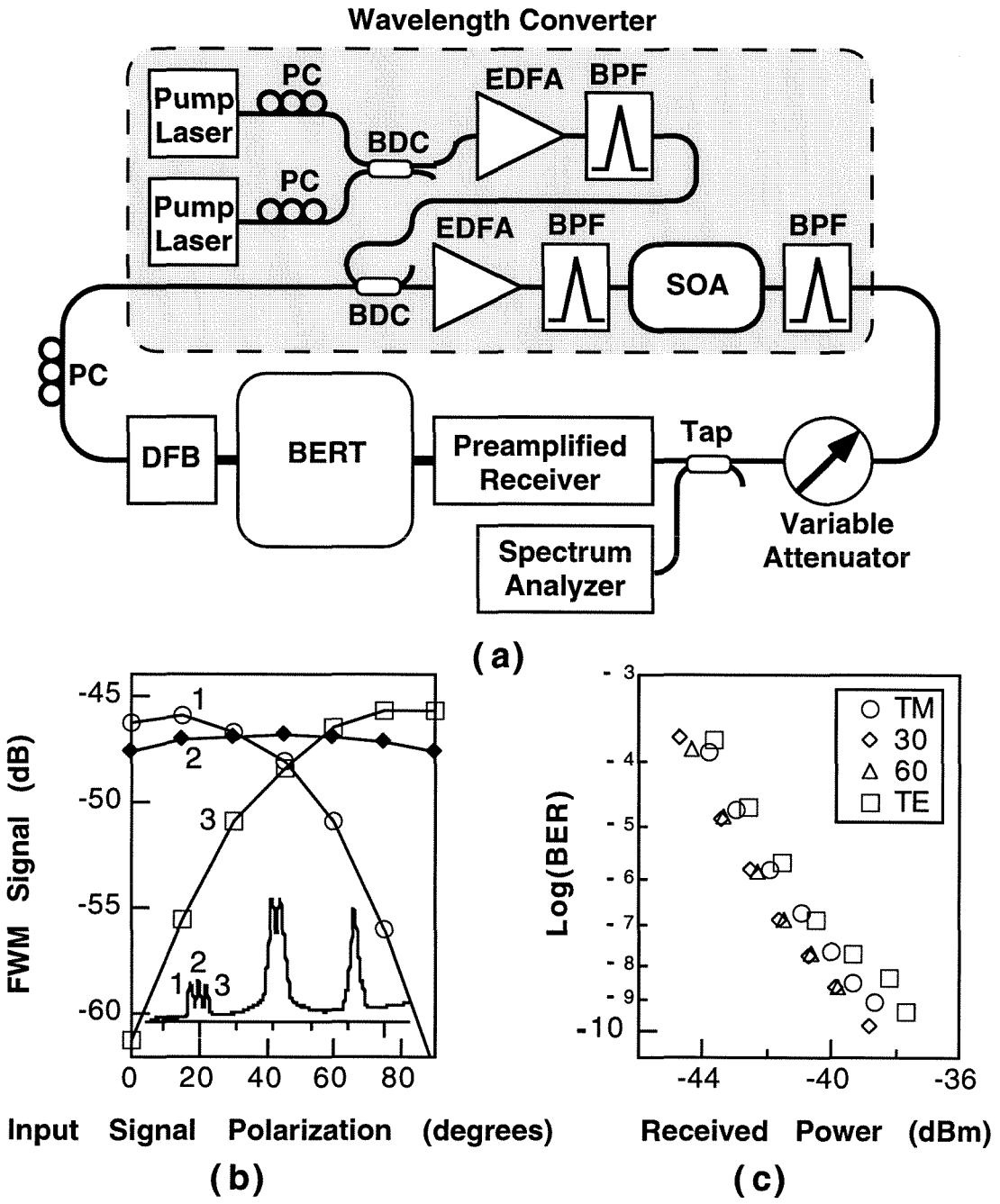

Figure 5.4: (a) Experimental setup to characterize polarization independent performance (b) polarization dependence of the magnitude of the converted signal. Inset shows a typical SOA output (c) BER vs. received power performance for various input polarizations.

The converted signal power in the center peak is relatively polarization independent, varying by less than 1.5 dB over all input polarizations. Centering the BPF at the converter output over the polarization-independent signal gives an approximately polarization independent received power. Slightly offsetting the filter can actually compensate for the small asymmetry in the susceptibility tensor, by unequal suppression of the polarization dependent FWM converted signals.

Curves for BER versus received power for various input signal polarizations are shown in Figure 5.4(c). Optimal performance is obtained for an input signal polarized at 45 degrees. The poorest performance is obtained for a TE polarized input signal. Over the entire range of input polarizations characterized, there is a maximum penalty of 1.5 dBs in received power. So with the modification to a dual-pump configuration, SOA FWM wavelength converters are able to provide nearly polarization independent performance.

Bibliography

[1] J. M. Wiesenfeld and B. Glance, "Cascadability and fanout of a semiconductor optical amplifier wavelength shifter," IEEE Photon. Technol. Lett., vol. 4, pp. 1168-1171, 1992.

[2] H. Yasaka, H. Sanjo, H.Ishii, Y. Yoshikuni, and K. Oe, "Repeated wavelength conversion of 10-Gbit/s signals and converted signal gating using wavelength-tunable semiconductor lasers," J. Light. Tech. vol. 14, 1042-1047, 1996.

[3] R. J. S. Pederson, M. Nissov, B. Mikkelsen, H. N. Poulsen, K. E. Stubaker, M. Gustavsson, W. van Berlo, and M. Janson, "Transmission through a cascade of 10 all-optical interferometric wavelength converter spans at 10 Gbit/s," Electron. Lett., vol. 32, pp. 1034-1035, 1996.

[4] D. F. Geraghty, R. B. Lee, and K. J. Vahala,"Cascaded wavelength conversions using four-wave mixing in semiconductor optical amplifiers," *Optical Fiber Communication Conference*, Dallas, Texas, February 16-21, 1997, paper WH6.

[5] D. F. Geraghty, R. B. Lee, and K. J. Vahala, "Cascaded wavelength conversions by four-wave mixing in semiconductor optical amplifiers at 10 Gb/s," *OSA Trends in Optics and Photonics Series*, vol. 12, 1997.

[6] E. Desurvire, *Erbium-Doped Fiber Amplifiers: Principles and Applications*, Wiley-Interscience, 1994.

[7] R. M. Jopson and R. E. Trench, "Polarization independent phase conjugation of lightwave signals," *Electron. Lett.*, vol. 29, pp. 2216-2217, 1996.

[8] K. Inoue, "Polarization independent wavelength conversion using fiber four-wave mixing with two orthogonal pump lights of different frequencies," *J. Lightwave Tech.*, vol. 12, pp. 1916-1920, 1994.

[9] R. Paiella, G. Hunziker, J. Zhou, K. J. Vahala , U. Koren, and B. I. Miller, "Polarization properties of four-wave mixing in strained semiconductor optical amplifiers and application to pump suppression," *IEEE Photon. Technol. Lett.*, vol. 8, pp. 773-775, 1996.

[10] G. Hunziker, R. Paiella, D. F. Geraghty, K. J. Vahala, and U. Koren, "Polarization-independent wavelength conversion at 2.5 Gbit/sec by dual-pump four-wave mixing in a strained semiconductor optical amplifier," *IEEE Photon. Technol. Lett.*, vol. 8, pp. 1633-1635, 1996.

[11] M. A. Newkirk, B. I. Miller, U. Koren, M. G. Young, M. Chen, R. M. Jopson, and C. A. Burns, "1.5 μm multi-quantum-well semiconductor optical amplifer with tensile and compressively strained wells for polarization-independent gain," *IEEE Photon. Technol. Lett.*, vol. 5, pp. 406-408, 1993.

[12] N Park, JW Dawson, and KJ Vahala, "All fiber, low threshold, widely tunable single-frequency, erbium-doped fiber ring laser with a tandem fiber Fabry-Perot filter," *Appl. Phys. Lett.*, vol. 59, pp. 2369-2371, 1991.

Chapter 6

Dispersion Compensation

6.1 Introduction

Most of the optical fiber utilized world-wide is non-dispersion shifted fiber, with its zero dispersion point near 1.3 μm. The successful development of EDFAs has prompted the use of 1.55 μm lasers for long haul links. With EDFAs properly placed in the link, the primary limiting factor to achievable transmission distance becomes signal distortion due to chromatic dispersion from propagation in the optical fiber.

Intrinsic to the process of wavelength conversion by FWM is spectral inversion of the input signal. Yariv *et al.* [1] proposed mid-span spectral inversion (MSSI) to compensate for chromatic dispersion in single-mode fiber. This process is shown in Figure 6.1. The average wavelength of a modulated signal will vary in time, with its variance being dependent on the specific pattern of modulation. The dispersive fiber medium will cause the different spectral components to propagate at different velocities. This will distort the signal as it propagates down a length of fiber. Wavelength

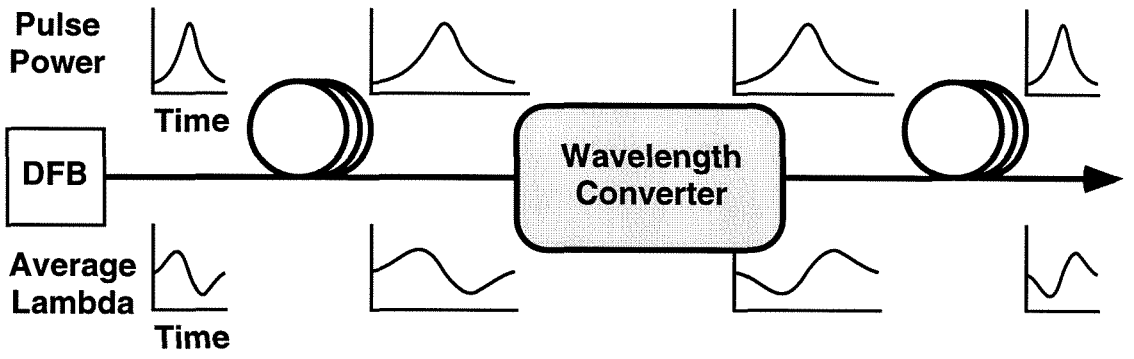

Figure 6.1: MSSI as a mechanism for dispersion compensation.

conversion in the middle of a link generates a spectral inversion of the signal while leaving the pulse shape unaffected. With the spectrally inverted copy, chromatic dispersion now works for you as the signal propagates a second identical length of fiber, and the signal will reshape itself.

Demonstrations have utilized both SOA [2, 3] and fiber [4] FWM wavelength converters to perform the MSSI for dispersion compensation, with impressive results. Ellis *et al* showed 40 Gbit/s transmission over 202 km of non-dispersion shifted fiber with a MSSI for a single channel/standard fiber record bit-rate-distance product of 8.1 Tbit/s km.

6.2 Time Resolved Spectral Analysis

6.2.1 Experimental Setup

To evaluate the performance of our FWM SOA wavelength converter as a spectral inverter, we perform time resolved spectral analysis (TRSA), shown in Figure 6.2 [5]. This has been demonstrated as an effective method for evaluating the spectral characteristics of a modulated laser [6]. By passing the signal through a narrow BPF before detection, the signal's spectral shape as a function of time can be determined. For this experiment, we directly drive the laser at 10 Gb/s. This produces a large amount of chirp on the signal, giving us more to look at. We utilize the monochrometer output of an optical spectrum analyzer for the narrow BPF. Its bandwidth of 0.08 nm is not optimal, but it provides superior stability. The center wavelength of the filter is stepped by 0.005 nm over the entire spectral width of the signal for each measurement. The filtered signals are detected for each step, using the preamplified receiver without the ac-coupled electrical amplifier so as to maintain the dc information of the experiment. These signals are then analyzed with a microwave transition analyzer.

This TRSA is performed both for signals directly from the laser and for signals that have undergone a wavelength conversion. The pump laser in the converter is set to have a P/Q ratio of 6 dB and to provide a 6 nm shift, approximately optimal conditions for the 10 Gb/s conversion.

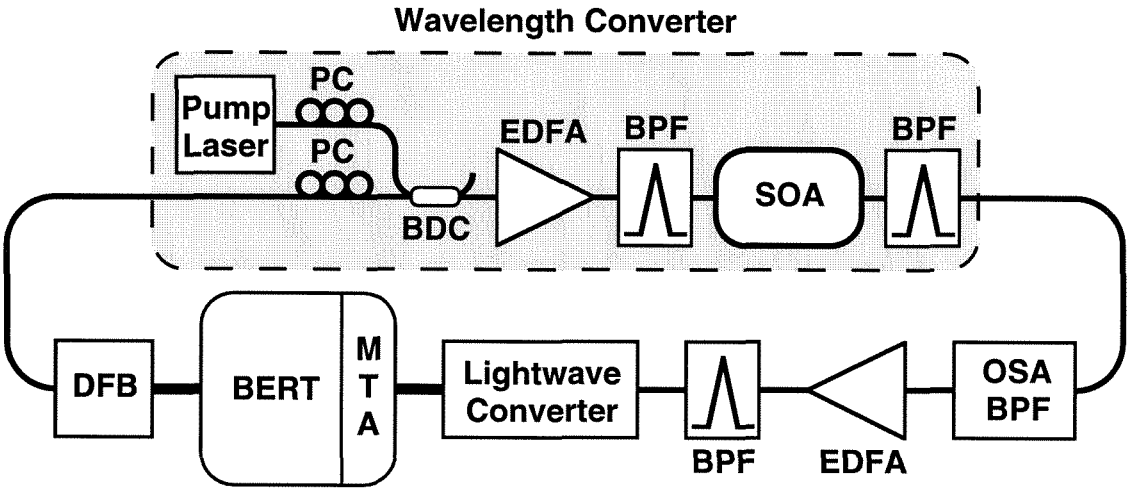

Figure 6.2: Experimental setup for TRSA of converted signals

6.2.2 Discussion of Results

The results of the analysis for the pattern 1111 0000 are shown in Figure 6.3. The upper panel shows the complete, unfiltered bit pattern. The middle two panels show TRSA contour plots, contour plots of constant power with time and wavelength as the x and y axes, respectively. These plots clearly demonstrate the spectral inversion intrinsic to the conversion. The shape of these contours is broadened in the wavelength direction by the non-optimal width of the narrow BPF. We are unable to deconvolve the filter shape from the data taken due to the noise. The contour plots are still informative, clearly showing the spectral inversion that occurs and revealing a broadening of the spectral shape by the conversion process.

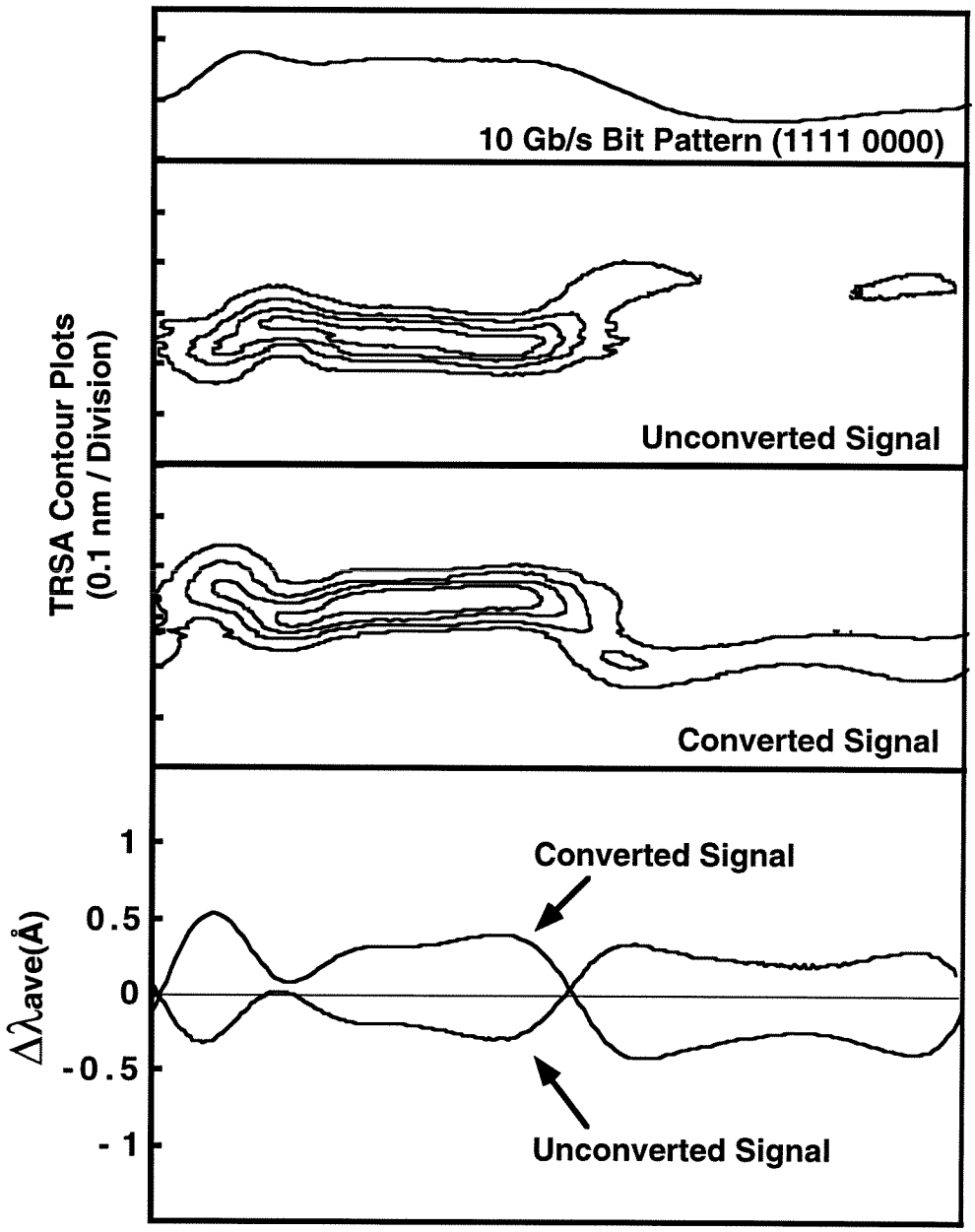

Figure 6.3: TRSA of (1111 0000) 10 Gb/s data signal. Upper panel shows complete data patterm. Middle two panels show TRSA contour plots of constant power. Bottom panel shows time dependence of the average wavelength.

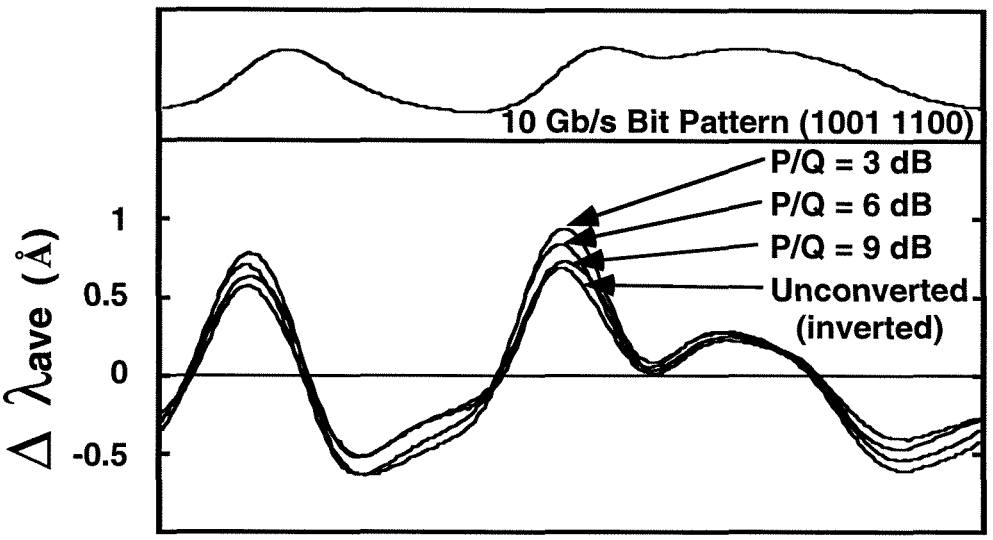

Figure 6.4: Average wavelength of (1001 1100) 10 Gb/s data signal at various P/Q and of the unconverted signal, inverted for comparison. Upper panel shows complete data patterm.

For a more quantitative analysis, the average wavelength of the signal is calculated at each point in time [7]. This is shown in the lower panel of Figure 6.3. Due to the nearly symmetrical shape of the power spectrum of the signal at any specific point in time, the average wavelength calculations will be almost unaffected by the non-optimal narrow BPF width. Again, the spectral inversion is evident. The average wavelength also clearly shows both the adiabatic and transient chirp. Also, we are able to calculate the change in the span of the average wavelength. For the pattern presented the span increased by 0.029 nm, or almost 50% as the wavelength conversion is introduced. For all the patterns tested, the span increased by between 0.005 and 0.05 nm, or about 5 to 44%.

This increase in the span of average wavelength is most likely due to additional

chirp introduced by the SOA as its gain saturation responds to the modulated input. The magnitude of this effect will be dependent upon the amount of the input signal that is modulated, or the P/Q. This is shown in Figure 6.4 for a (1001 1100) pattern. The average wavelength is shown for P/Q of 3, 6, and 9 dB and compared to the inverted average wavelength of the unconverted signal. The span of the average wavelegnth increases by 0.0054, 0.0274, and 0.0378 nm, corresponding to 5, 23, and 31.5 % changes, for P/Q of 3, 6, and 9 dB. Although the spectral inversion that occurs during FWM in SOAs is non-ideal, the resulting spectral inversion is good enough for dispersion compensation in optical fibers at larger P/Q.

6.3 Mid-Span Spectral Inversion

Figure 6.2(a) shows a diagram of the system used to demonstrate dispersion compensation by MSSI. The BERT directly modulates a DFB at 10 Gb/s. This signal propagates through 60 km of standard, non-dispersion shifted, single-mode fiber. It is then amplified to compensate for propagation losses. The signal is spectrally inverted by the wavelength converter at this point. The converter is set for a P/Q ratio of 8.8 dB and a shift of 6 nm. The spectrally inverted signal is then amplified and sent through another 60 km of standard fiber. Finally, the signal is detected with the preamplified receiver.

Eye diagrams at various points in the system are shown in Figure 6.2(b). The eye diagrams are taken both for a PRBS pattern and a 1001 1100 pattern. The original signal shows a clean PRBS eye, the main imperfection being a small amount

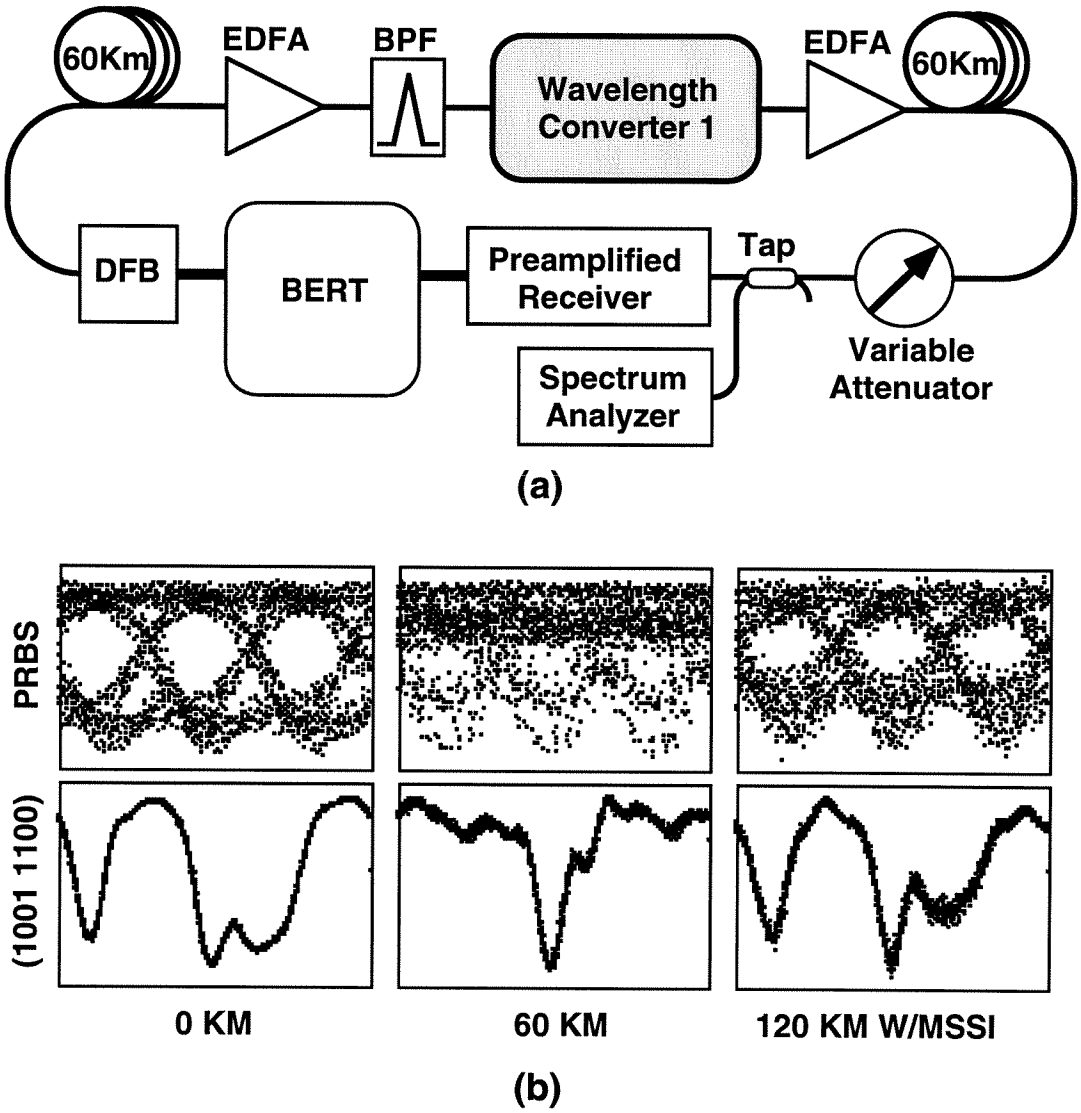

Figure 6.5: (a) Experimental setup for dispersion compensation by MSSI (b) PRBS and (10011100) eye diagrams at various points in the system

of ringing at the turn-on. After propagating through 60 km of standard single-mode fiber, chromatic dispersion has caused severe distortion of the signal. The single "1" has completely disappeared, and the three "1"s have compressed into a single peak approximately one bit long.

Introducing MSSI between the two 60 km segments of fiber allows for dispersion compensation as the signal propagates through the second 60 km segment of fiber. The wavelength converter is inserted after the first 60 km segment of fiber. Its input signal does not resemble the original signal at all. As the converted signal propagates through the second 60 km segment of fiber, the signal regenerates itself and is easily recovered at 120 km. The eye shows minimal distortion of the original signal and we are able to do error-free detection for over 2 minutes.

Bibliography

[1] A. Yariv, D. Fekete, and D. M. Pepper , "Compensation for channel dispersion by nonlinear optical phase conjugation," *Optics Lett.*, vol. 4, pp. 52-54, 1979.

[2] M. C. Tatham, X. Gu, L.D. Westbrook, G. Sherlock and D. M. Spirit, "Transmission of 10 Gb/s directly modulated DFB signals over 200 km standard fibre using mid-span spectral inversion," *Electron. Lett.*, vol. 30, pp. 1335-1336, 1994.

[3] A. D. Ellis, M. C. Tatham, D. A. O. Davies, D. Nesset, D. G. Moodie and G. Sherlock, "40 Gbit/s transmission over 202 km of standard fibre using midspan spectral inversion," *Electron. Lett.*, vol. 31, pp. 299-301, 1995.

[4] S. Watanabe, T. Naito, and T. Chikama, "Compensation of chromatic dispersion in a single-mode fiber by optical phase conjugation," *IEEE Photon. Technol. Lett.*, vol. 5, pp.92 - 95, 1993.

[5] D. F. Geraghty, R. B. Lee, K. J. Vahala, M. Verdiell, M. Ziari, and A. Mathur, "Time resolved spectral analysis of phase conjugation by four-wave mixing in semiconductor optical amplifiers," *Conference on Lasers and Electro-Optics*, Baltimore, Maryland, May 18-23, 1997, paper CTuH6.

[6] R. A. Linke,"Modulation induced transient chirping in single frequency lasers," *IEEE J. Quantum Electron.*, vol. QE-21, pp. 593-597, 1985.

[7] T. L. Koch, R. A. Linke, "Effect of nonlinear gain reduction on semiconductor laser wavelength chirping," *Appl. Phys. Lett.*, vol. 48, pp. 613-615, 1986.

Chapter 7

Additional Demonstrations

7.1 Multi-Channel Operation

7.1.1 Introduction

A significant potential advantage of FWM over cross-gain and cross-phase saturation for wavelength conversion is the capability to perform simultaneous multi-channel conversions without first using expensive demultiplexing equipment to separate the incoming signals. However, cross-gain saturation provides the opportunity for crosstalk between the input signals and, consequently, signal degradation [1].

7.1.2 Experimental Setup

We perform an experimental characterization of the multi-channel capabilties of FWM SOA wavelength converters. The setup is shown in Figure 7.1(a). We begin with 2 input signals: 2 DFBs directly modulated at 2.5 Gb/s with an NRZ PRBS, one with data and one with databar. They each go through individual PCs and then

are combined in a 50/50 BDC before being input into the wavelength converter. The two signals begin as inverted data streams. They then travel through different lengths of fiber, delaying one signal by several bits, before being combined. Generating the signals through this process, we can then assume that they are approximately independent NRZ PRBS signals. The two input signals are separated in wavelength by 1.5 nm. Due to the wavelength dependence in the gain of the high-power EDFA in the wavelength converter, the powers of the input signals are offset so as to give identical P/Q ratios at the SOA output. The pump wavelength is chosen such that the outer channel, Channel 1, goes though a 9 nm conversion and the inner channel, Channel 2, goes through a 6 nm conversion. Detection is done with the same method as described in Chapter 4.

7.1.3 Discussion of Results

The wavelength converter we are using does not utilize any expensive demultiplexing equipment to separate the input signals before conversion. Maintaining a large P/Q, so that the input signals do not significantly contribute to the gain saturation of the high-power EDFA and the SOA, it is possible to do simultaneous wavelength conversion of both channels. Figure 7.1(b) shows the BER performance of 2 channels simultaneously converted with P/Qs of 18 dB. Both channels show a very linear performance of identical sensitivity with negligible flooring. The sensitivity of both converted signals is within 0.5 dB of that for a single channel conversion with the same P/Q.

This performance is only achievable for a large P/Q. Through the mechanism of

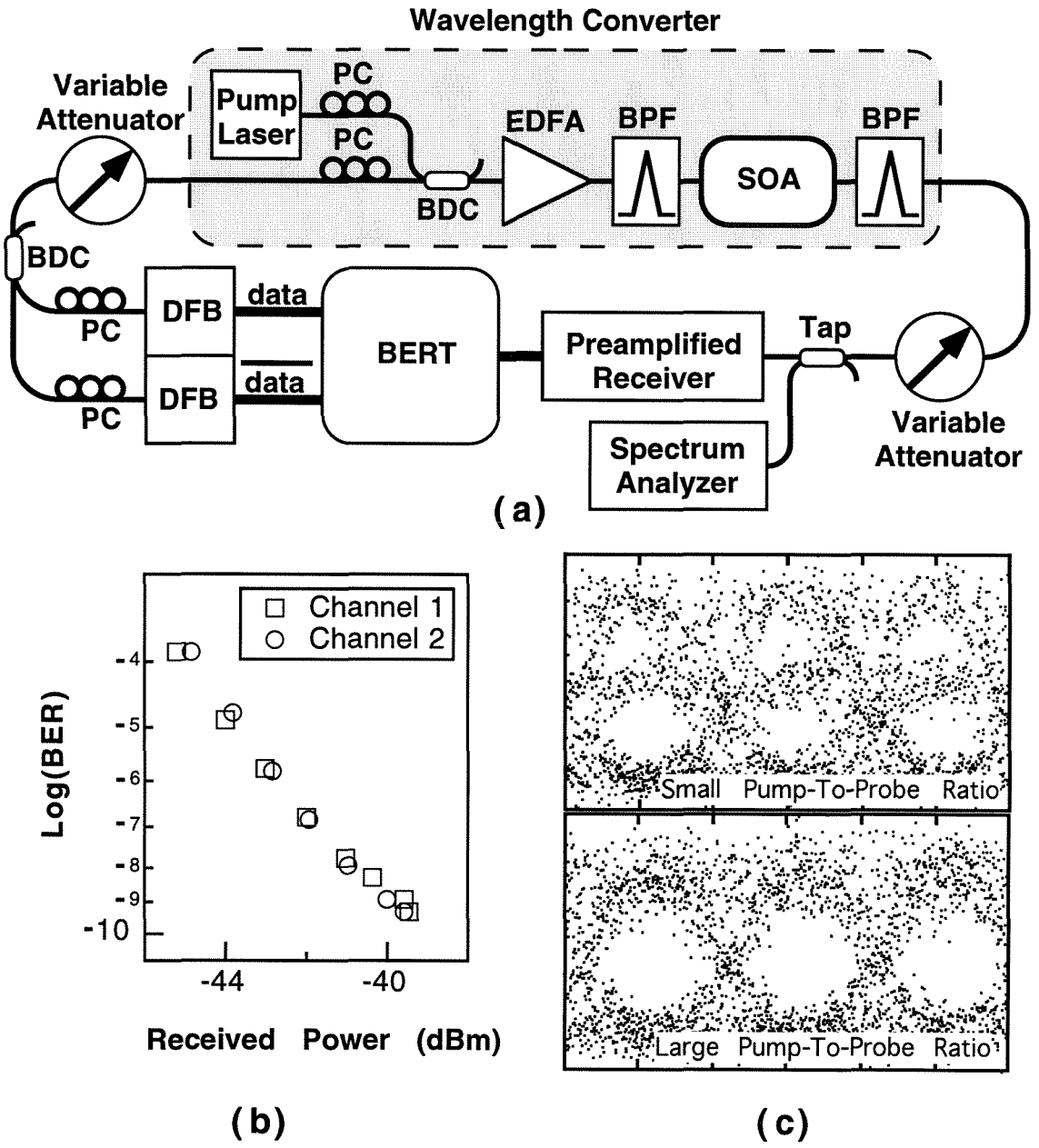

Figure 7.1: (a) Experimental setup for the demonstration of multi-channel operation. (b) BER vs. received power performance for the two channels at a large P/Q of 18 dB. (c) Eye diagrams taken for Small and large P/Q.

cross-gain saturation, both the signal and the noise of a channel can be imposed upon the gain of the SOA and therefore on the pump. This effect strengthens with decreasing P/Q. As previously mentioned, it can be easily seen in a single channel conversion. For P/Qs of < 5 dB, it is possible to do measurements with BER $< 10^{-9}$ by detecting only the pump.

Since both the pump power and the gain affect the magnitude of the converted signal, cross-gain saturation imposes the signal and the noise of one channel onto the converted signal of the other. This is evident in the eye shown in the upper panel of Figure 7.1(c), taken during multi-channel operation with a P/Q of 7.4 dB. Here we see that the eye has two "1" levels, the higher and lower "1" levels corresponding to when the channel not being detected is a "0" and a "1", respectively. Simple cross gain calculations predict the eye closure of 40% that occurs from the introduction of these two levels. As P/Q increases, the reduction in eye height disappears as the contribution to gain saturation by the input signals becomes negligible. This is evident in the eye shown in the lower panel of Figure 7.1(c), taken for a P/Q of 16 dB.

For large P/Q, multi-channel operation provides excellent performance with minimal degradation compared to single channel operation. As P/Q decreases, cross-gain saturation caused by the input signals causes a reduction in the eye height of the converted signal. Due to the reduction of the eye height, the sensitivity of the converted signal begins to rise for P/Q above 15 dB.

7.2 Dynamic Routing

7.2.1 Introduction

One of the exciting possibilities for wavelength conversion is dynamic channel routing. With a wavelength converter providing tunable wavelength shifts and fixed wavelength selective filters, wavelength routing and add/drop multiplexers can be implemented. There are other methods for dynamic channel routing which do not require wavelength conversion [2]. However, for routing between levels in a system these methods would not offer the prevention of wavelength blocking and the decoupling of interconnection schedulers from global knowledge of the system, benefits offered by wavelength conversion routers.

7.2.2 Experimental Setup

The experimental setup to demonstrate dynamic routing is shown in Figure 7.2(a). The dynamic router used is identical to the wavelength converter described in Chapter 3, with two modifications. No ASE prefilter is used merely because one was not available at the time of the experiment. Additionally, there is a 1x8 demultiplexer replacing the BPF at the SOA output. The demultiplexer used is a fiber pigtailed $LiNbO_3$ device. Its channels are 0.8 nm wide; they are separated by 4.8 nm, and they each have about 6 dB throughput loss. Due to the fixed channels of the demultiplexer and wavelength of our probe, and due to the limitation on wavelength shift imposed by conversion efficiency, we are only able to access two of the channels making it effectively a 1x2 demultiplexer. An isolator is used after the demultiplexer to prevent

reflection of backward traveling ASE from the EDFA in our preamplified receiver.

External to the dynamic router, completing the system, the input signal is a DFB directly modulated at 2.5 Gb/s NRZ PRBS. Detection of the routed signal is identical to that described in Chapter 4.

7.2.3 Discussion of Results

Using the demultiplexer at the wavelength converter's output, we are able to route the signal to either of the fiber outputs simply by tuning the pump wavelength to control the converted signal's wavelength. We then detect both fiber outputs individually, tuning the BPF in the preamplified receiver to the proper wavelength.

The BER versus received power data, shown in Figure 7.2(b), reveals only a small difference of about a dB between the two fibers. The fiber that corresponds to the longer shift actually has lower received power for BERs $> 10^{-10}$ due to the fact that its converted signal wavelength sees superior performance from the preamplified receiver. For higher BER the curve has floored, due to the smaller OSNR resulting from the larger shift.

With a more optimal demultiplexer design, and with the increased spectral range provided by the addition of the ASE prefilter, it would be a stright-forward extension of this work to demonstrate routing to between 8 to 18 fibers of 10 Gb/s signals.

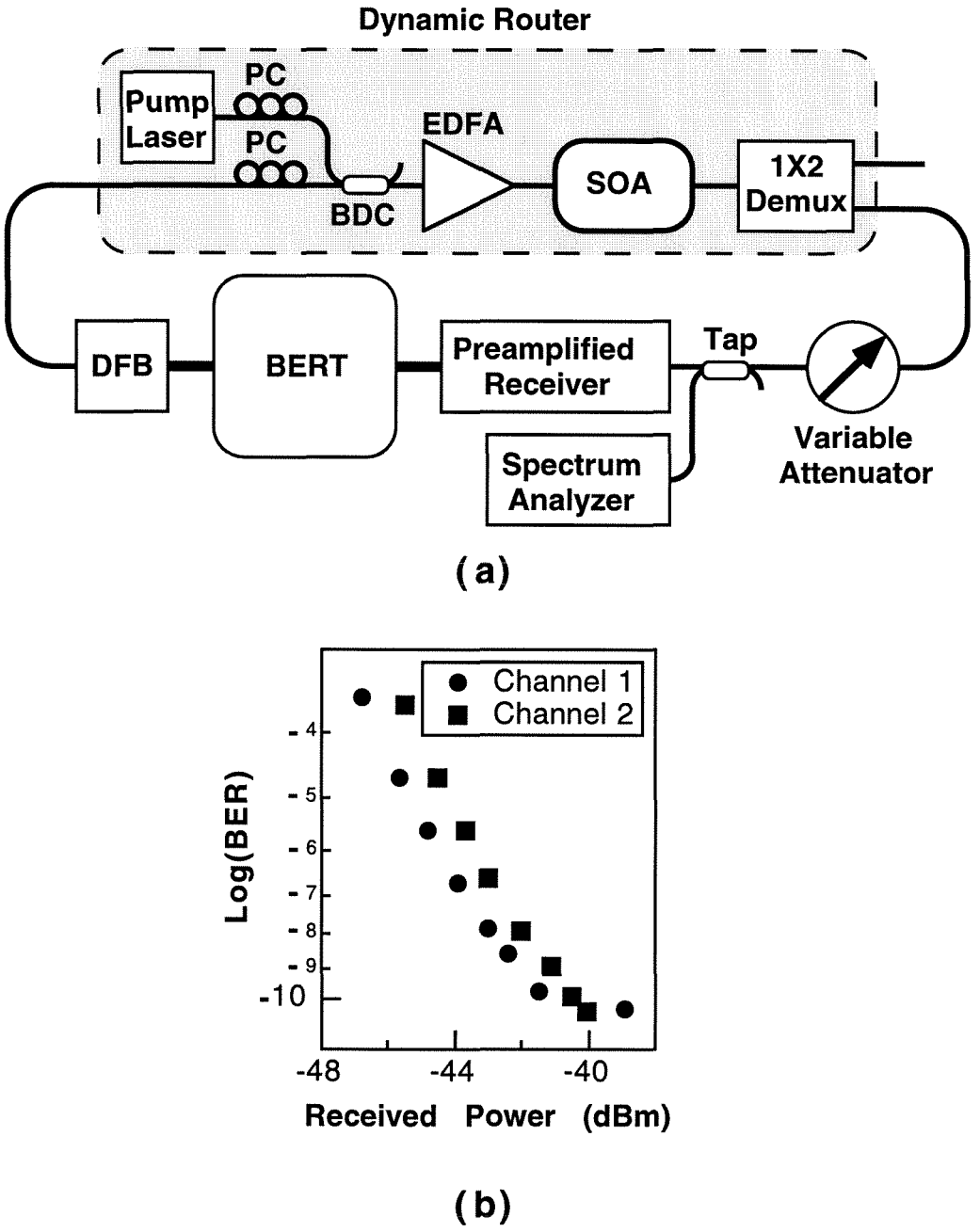

Figure 7.2: (a) Experimental setup for the demonstration of dynamic routing. (b) BER vs. received power performance for the routed channels.

Bibliography

[1] J. P. R. Lacey, S. J. Madden, M. A. Summerfield, R. S. Tucker and A. I. Faris, "Four-channel WDM optical phase conjugator using four-wave mixing in a single semiconductor optical amplifier," *Electron. Lett.*, vol. 31, pp. 743 - 745, 1995.

[2] J. L. Jackel, M. Goodman, J. Gamelin, W. J. Tomlinson, J. Baran, C. A. Brackett, D. J. Fritz, R. Hobbs, K. Kissa, R. Ade, and D. A. Smith, "Demonstration of simultaneous and independent switching of eight wavelength channels with 2 nm spacing using a wavelength-dilated acousto-optic switch," *IEEE Lasers and Electro-Optics Society 1995 Annual Meeting*, San Francisco, CA, 1995, paper PD1.2.

Chapter 8

Microcavity Laser

8.1 Motivation

The potential for erbium-doped fiber lasers in communication and sensing systems has received much attention lately due to these lasers' narrow linewidth, broad tuning range, and intrinsic fiber compatibility. Many laser structures have been demonstrated and characterized. However, implementation of these structures in communication systems is not yet promising due to their size and complexity [1, 2, 3, 4], or their limited tuning range [5]. Here we demonstrate an all-fiber, microcavity, erbium-doped fiber laser. Its connectorized construction is simple and compact and yields multimode operation, useful in some simple applications, with a threshold pump power of 15 mW.

8.2 Experimental Demonstration

The design of the desired fiber laser is shown in Figure 8.1(a). The fiber laser demonstrated is similar, except that it doesn't have piezo control of the air gap. It is identical in design to fiber Fabry-Perot filters previously reported [6]. The gain medium is a 1.75 cm segment of highly-doped erbium fiber (AT&T, 2000 ppm, 5 micron core diameter) encased in a double-ended, tungsten carbide ferrule with a flat polish. The outputs comprise two single mode fibers encased in tungsten carbide ferrules with flat polishes. The polished faces of the output fibers are coated with dielectric stack reflectors that are reflective ($R > 0.98$) for wavelengths around 1530 nm, corresponding to the gain maximum of the erbium fiber, but are transparent at the pumping wavelength of 980 nm. The three ferrules are aligned to form a linear cavity in a precision cylindrical sleeve. Pump power is coupled into the system using a 980/1550 fiber wavelength division multiplexer.

The laser is pumped at varying power levels and the output is monitored with an optical spectrum analyzer to determine the threshold. The results are shown in Figure 8.1(b), where the output power shown is the estimated sum of the power in all of the lasing modes. The deviation from linearity at high pump powers is primarily due to power in lasing modes not included in the sum of the total power. The laser has a threshold of about 7 mW of in-line pump power. Approximately half of the in-line pump power is absorbed in the short erbium segment (at a pump power of 5 mW). The high pump power as well as low output power are most likely due to large cavity losses, which can be decreased by improved ferrule polishing and alignment.

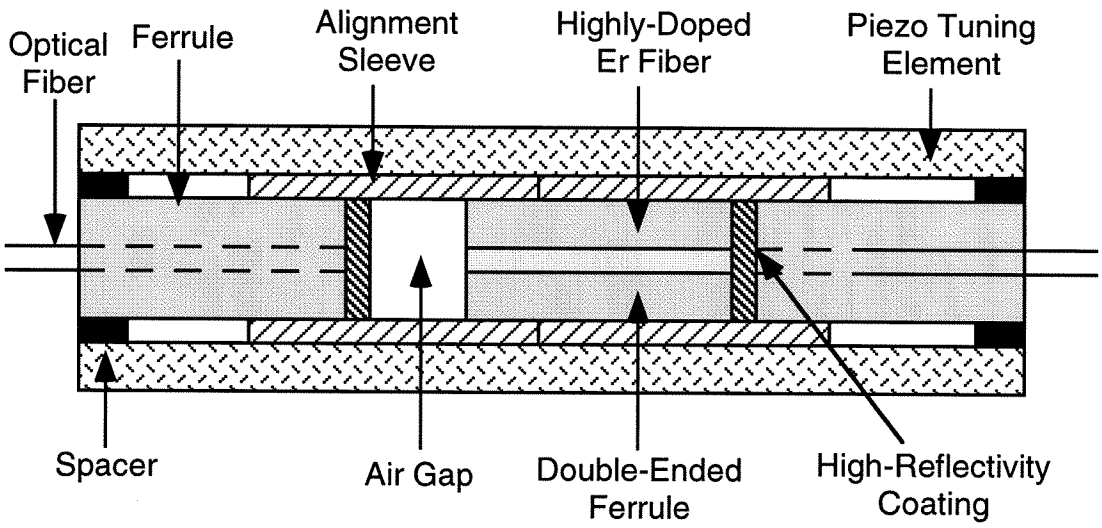

(a)

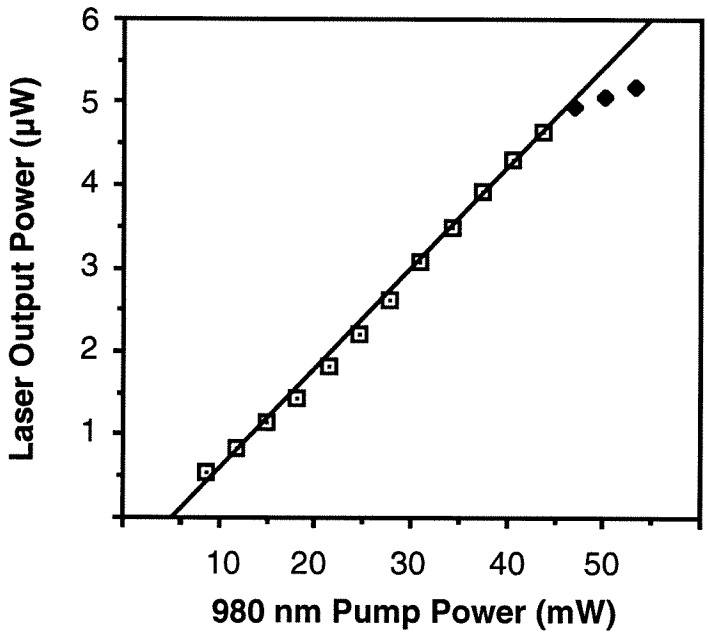

(b)

Figure 8.1: (a) Proposed design of microcavity erbium-doped fiber laser. (b) Luminescence vs. pump power performance.

Lasing emission spans 2.1 nm centered around 1531 nm. The power spectrum of the lasing modes exhibits several distinct peaks. As the in-line pump power is changed, the relative intensities of the lasing modes also change. These effects are most likely due to unintended coupled-cavity effects in our design resulting from parasitic reflection at the erbium fiber-air interface. This effect could, in future devices, be included by design in order to control which of the cavity's longitudinal modes will lase. This technique is commonly used for control of lasing modes in cleaved coupled-cavity lasers [7].

The lasing modes are too closely spaced to be resolved by the optical spectrum analyzer, but they can be resolved by use of optical heterodyne detection. The laser output is combined with the output of a stabilized single frequency erbium fiber ring laser [3] using a 50/50 BDC. The signals are mixed by detection with a high-speed pin photodiode. The photocurrent is amplified and then monitored with an electronic spectrum analyzer to detect beating between the single line of the ring laser and the multiple lines of the microcavity laser.

The photocurrent power spectrum displays multiple lines, revealing two polarization states. As the polarization of the ring laser was rotated using an intracavity polarization controller, the amplitude of half of the beat signals would rise while the amplitude of the other half would fall, confirming that each set of beat signals are from different polarization states. The laser's longitudinal modes are observed to have a 5.72 GHz separation for both polarizations.

A single beat signal between the a microcavity laser line and the line of the ring

laser reveals the microcavity laser linewidth. The ring laser's linewidth is known to be less than 4 kHz, so the width of the observed beat signal is almost entirely due to the linewidth of the microcavity laser line. Individual longitudinal modes of the microcavity laser are observed to have a linewidth of approximately 250 kHz.

8.3 Subsequent Work

We have demonstrated an all-fiber, microcavity, erbium-doped fiber laser. The laser's linewidth, longitudinal mode spacing and output power have been characterized. An external amplification section could easily be implemented to improve output power. Reduction of cavity losses will allow the addition of piezoelectric cavity length control, as demonstrated in [7]. This will create tuning capabilities and allow simple temperature stabilization. Furthermore, utilization of coupled cavity effects should offer control of the number of lasing longitudinal modes.

Following the successful completion of this work, Hsu *et al.* demonstrated the desired laser structure. Benefiting from superior polishing and alignment technologies developed in their fiber Fabry-Perot productization, and also from superior erbium-doped fiber not commercially available, they were able to demonstrate single line lasing, tunable over 4.52 nm [8].

Bibliography

[1] R. Wyatt, "High-power broadly tunable erbium-doped silica fibre laser," *Electron. Lett.*, vol. 25, pp. 1498-1499, 1989.

[2] P. F. Wysocki, M. J. F. Digonnet, and B. Y. Kim, "Electronically tunable, 1.55 μm erbium-doped fiber laser," *Opt. Lett.*, vol. 15, pp. 273-275, 1990.

[3] N. Park, J. W. Dawson, and K. J. Vahala, "All fiber, low threshold, widely tunable single-frequency, erbium-doped fiber ring laser with a tandem fiber Fabry-Perot filter," *Appl. Phys. Lett.*, vol. 59, pp. 2369-2371, 1991.

[4] G. A. Ball, W. W. Morey, and W. H. Glenn, "Standing-wave monomode erbium fiber laser," *IEEE Phot. Tech. Lett.*, vol. 3, pp. 613-61,5 1991.

[5] J. L. Zyskind, V. Mizrahi, D. J. DiGiovanni, and J. W. Sulhoff, "Short single frequency erbium-doped fibre laser," *Electron. Lett.*, vol. 28, pp. 1385-1387, 1992.

[6] J. Stone, L. W. Stulz,"Pigtailed high-finesse tunable fibre Fabry-Perot interferometers with large, medium and small free spectral ranges," *Electron. Lett.*, vol. 23, pp. 781-783, 1987.

[7] C. H. Henry and R. F. Kazarinov, "Stabilization of single frequency operation of coupled-cavity lasers", *IEEE J. Quantum Electron.*, vol. QE-20, pp. 733-744, 1984.

[8] K. Hsu and C. M. Miller,"Tunable erbium: Ytterbium fiber Fabry-Perot micro laser," *Optical Fiber Communication Conference*, San Jose, California, February 20-25, 1994, paper PD1.

Appendix A

Components for Converter Characterization

A.1 External Modulator

The equipment used external to the wavelength converter for the systems experiments was mentioned in the appropriate chapters. Some of the equipment warrants further clarification and discussion of its impact on the overall system performance.

In order to maximize the overall system performance for the spectral range characterization and cascaded converter demonstration at 10 Gb/s, the optical signal source utilized is an Ortel high-speed DFB modulated by a $LiNbO_3$ Mach-Zehnder external modulator. The specifications on the modulator are a driving voltage of 16 V peak-to-peak for a π phase shift, or a "0" to "1" transition. The BERT's maximum peak-to-peak voltage for the data output is 2 V. Therefore, an electrical amplifier is required. The only amplifier available that has a wide enough bandwidth provides a

peak-to-peak voltage of only 7 V. This results in incomplete modulation of the input signal. The dc bias operating is chosen by first maximizing the extinction ratio of the modulator output, and then by adjusting the dc bias around this point minimizing the BER for a given received power. This provides a modulation of approximately "0" to "0.5". Due to the $sine^2$ transfer function of the modulator, this introduces some distortion to the signal by rounding out the turning on and off near the "0" point. However, a similar signal distortion is introduced by the high-frequency electrical noise filtering in the electrical preamplifier, so degradation to the overall system performance should be negligible.

A.2 Preamplified Receiver

The pre-amplified receiver has a high-gain, low-noise EDFA at its input. The EDFA is followed by a 1 nm wide tunable BPF, DiCon model TF-1-1565-FC/APC-P-L-3. Although the ideal bandwidth of this BPF would be twice the bit-rate, this filter is narrow enough that it should introduce minimal degradation to the overall system performance [1]. The optically amplified signal is then detected and electrically amplified with a lightwave converter, Hewlett Packard Model HP 11982A, consisting of a PIN receiver and an electrical amplifier. This electrical signal is then amplified by an rf amplifier, Hewlett Packard Model HP 8347A for the 2.5 Gb/s experiments and Veritech Model VMA3K10P-124 for the 10 Gb/s experiments. High frequency noise is suppressed by the roll-off of the amplifier gain for 10 Gb/s experiments and by a standard SONET filter, Hewlett Packard Model HP 87441D, for experiments at 2.5

Gb/s. This receiver output is then split by a 10X coaxial probe at the BERT input in order to allow us to both look at the eye diagrams and do BER measurements.

A.3 EDFA Preamplifier

The EDFA preamplifier used in the preamplified receiver is a home-built module designed specifically for detecting the wavelength converted signals. The EDFA has very good performance, however, for the sake of simplicity and affordability it does have some limitations that affected the work presented in this thesis.

The design of the preamplifier, shown in Figure A.1(a), was driven by the desired specifications. The EDFA was to be used as a preamplifier for detection of the converted signals with the HP Lightwave Converter we had already purchased. For the converted signal powers we are able to achieve, we need the preamplifier to have gain of > 30 dB for input signals < 25 dBm with as small as possible a noise figure (NF). These two considerations determined the amplifier design.

In order to minimize the NF, the amplifier was designed as a two stage device. An isolator separating the two segments of erbium fiber will suppress the backward traveling ASE from the later part of the gain element, reducing the gain suppression at the start of the amplifier caused by ASE amplification. The isolator does not pass 980 nm light in either direction. This results in the necessity for the use of tandem WDMs to allow the 980 nm pump power to bypass the isolator so that the preamplifier can be pumped using a single pump laser.

Due to the degradation of the NF introduced by lossy elements, there is no isolator

on the input stage of the amplifier. This aspect limits the length of the first segment of fiber. With the 90 mW of pump power available, the erbium fiber (AT&T HE980) provides approximately 1 dB of gain per meter. In order to avoid lasing in the first gain segment from parasitic reflections, no longer suppressed by an isolator at the input, the length of the first segment is limited to 11 m. The total gain requirement of > 30 dB, along with the 1.1 dB per meter gain, then determines the length of the second gain segment to be 20 m.

This EDFA design offers excellent performance for its simplicity. The small signal gain for the EDFA is shown in Figure A.1(b). Over 40 dB of gain is available for small signals at the peak gain wavelength of 1532 nm. The small signal gain remains over 30 dB until around 1550 nm. This spectral dependence of the preamplifier performance is what has negated the value of baseline, unconverted signal data for the work presented in this thesis. Comparing the converted signal performance to the unconverted signal performance is deceiving in that the two signals see different performance from the preamplifier in the receiver since they are at different wavelengths. This is clearly seen in Figure 5.1(b), where the converted signal shifted down 5 nm shows a dB in sensitivity over the unconverted signal.

The NF for the preamplifier was determined by a simple program in Labview. Using a Hewlett Packard optical spectrum analyzer, model HP 70950A, spectrum traces were saved for the small signal input and output of the EDFA. The NF is then calculated using the equation [2]

$$NF = \frac{N_{out} - G\,N_{in}}{h\nu\,G\,B_w} + \frac{1}{G}\ , \tag{A.1}$$

where B_w is the resolution bandwidth of the OSA, G is the gain of the EDFA, ν is the frequency of the input signal, and N_{in} and N_{out} are the background ASE levels of the input and output signal, respectively, measured at a wavelength $2B_w$ away from the input peak. The NF for the preamplifier is shown in Figure A.1(c). Varying by about 1 dB for wavelengths from 1530 to 1560 nm, its worse performance is 4.5 dB.

Although the amplifier design offers excellent performance, it is non-ideal. A few modifications could have been implemented in order to improve the performance, however they were prohibitive due to cost or complexity. The overall gain and NF could have been improved by using two 980 nm pumps, one to pump each gain segment. Since the first segment is short enough that we can assume that it is fully inverted, the first stage would be backward pumped, eliminating the need for the WDM at the input of the EDFA. This would remove a lossy element, improving the NF of the amplifier. The second gain segment would again be forward pumped, since there is already enough gain and the forward pumping offers better NF performance for this longer section which is not fully inverted. Having a pump laser dedicated to the second section would provide it with more pump power and therefore improve its gain.

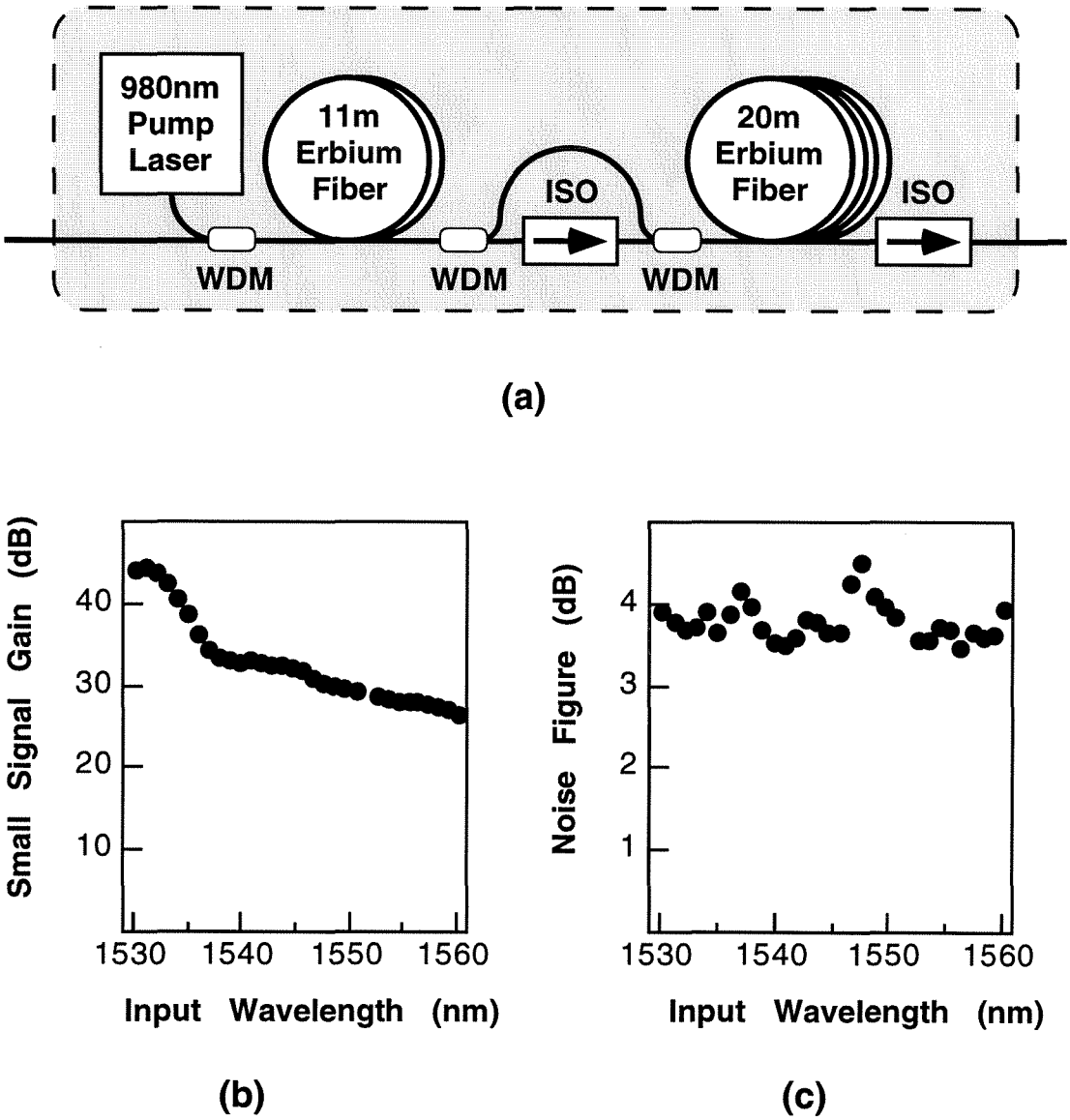

Figure A.1: EDFA premplifier(a) schematic, (b) small signal gain and (c) noise figure.

Bibliography

[1] P. M. Gabla, E. Leclerc, and C. Coeurjolly,"Practical implementation of a highly sensitive receiver using an erbium-doped fiber preamplifier," *IEEE Phot. Tech. Lett.*, vol. 3, pp. 727-729, 1997.

[2] E. Desurvire, *Erbium-Doped Fiber Amplifiers: Principles and Applications*, Wiley-Interscience, 1994.